

Article

Origin and Geological Implications of Monzogranites and Rhyolitic Porphyries in the Wunugetu Porphyry Copper–Molybdenum Deposit, Northeast China: Evidence from Zircon U–Pb–Hf Isotopes and Whole-Rock Geochemistry

Qingshuang Wang^{1,2}, Yanchen Yang^{1,*}, Qiulin Fu³, Zhongyue Zhang⁴, Xiaodan Guo⁵, Taotao Wu², Lu Chai², Yongheng Zhou² and Yonghai An⁵

- ¹ College of Earth Sciences, Jilin University, Changchun 130061, China; wangqingshuang1988@163.com
² Shenyang Geological Survey Center of China Geological Survey, Shenyang 110034, China; wutaotao@mail.cgs.gov.cn (T.W.); chailu@mail.cgs.gov.cn (L.C.); zhoyongheng@mail.cgs.gov.cn (Y.Z.)
³ Liaoning Province Institute of Geology and Mineral Resources Co., Ltd., Shenyang 110034, China; woshifuqiulin@163.com
⁴ Liaoning Earthquake Agency, Shenyang 110031, China; 13390583679@163.com
⁵ Liaoning Province Geology and Mineral Group Energy Geology Co., Ltd., Shenyang 110032, China; guoxiaodan63@163.com (X.G.); liwaca@163.com (Y.A.)
* Correspondence: yyc@jlu.edu.cn



Citation: Wang, Q.; Yang, Y.; Fu, Q.; Zhang, Z.; Guo, X.; Wu, T.; Chai, L.; Zhou, Y.; An, Y. Origin and Geological Implications of Monzogranites and Rhyolitic Porphyries in the Wunugetu Porphyry Copper–Molybdenum Deposit, Northeast China: Evidence from Zircon U–Pb–Hf Isotopes and Whole-Rock Geochemistry. *Minerals* **2024**, *14*, 310.

<https://doi.org/10.3390/min14030310>

Academic Editor: Massimo D'Antonio

Received: 22 January 2024

Revised: 13 March 2024

Accepted: 13 March 2024

Published: 15 March 2024



Copyright: © 2024 by the authors. Licensee MDPI, Basel, Switzerland. This article is an open access article distributed under the terms and conditions of the Creative Commons Attribution (CC BY) license (<https://creativecommons.org/licenses/by/4.0/>).

Abstract: The Wunugetu deposit, a large-scale porphyry copper–molybdenum deposit, is located in the southern Erguna block. Its ore bodies are primarily found within monzogranites, granite porphyries, and biotite monzogranites. Additionally, the deposit contains late-stage intrusive dykes of rhyolitic porphyries. This study examined the deposit's monzogranites and rhyolitic porphyries using lithogeochemistry, zircon U–Pb dating, and Hf isotopic analysis. The main findings include: (1) Zircon U–Pb dating showed that the monzogranites formed around 209.0 ± 1.0 Ma, whereas the rhyolitic porphyries in the northern portion formed around 170.49 ± 0.81 Ma, suggesting magmatic activity in the deposit spanned from the Late Triassic to the Middle Jurassic. (2) The monzogranites exhibited high silicon content (73.16–80.47 wt.%) and relatively low aluminum content (10.98–14.37 wt.%). They are enriched in alkalis (content: 3.42–10.10 wt.%) and deficient in magnesium and sodium, with aluminum saturation indices (A/CNK) ranging from 1.1 to 2.9. In addition, the monzogranites are enriched in large-ion lithophile elements (LILEs) such as Rb, K, and Ba and deficient in high-field-strength elements (HFSEs) like Nb, P, and Ti. (3) The monzogranites have low $Zr + Nb + Ce + Y$ contents of $(151.3\text{--}298.6 \text{ ppm}) \times 10^{-6}$ and $10,000 \times Ga/Al$ ratios varying between 1.20 and 2.33, suggesting that they are characteristic of I-type granites. (4) Positive zircon $\epsilon Hf(t)$ values ranging from +0.3 to +7.6 in both rhyolitic porphyry and monzogranite samples, increasing with younger emplacement ages, imply that the deposit's rocks originated from magmatic mixing between mantle-derived mafic magmas and remelts of the juvenile crust. Considering these results and the regional geological evolution, this study proposes that the Wunugetu deposit was formed in an active continental margin setting and was influenced by the Late Triassic–Middle Jurassic southeastward subduction of the Mongol–Okhotsk Ocean.

Keywords: Cu–Mo deposit; lithogeochemistry; I-type granite; Mongolia–Okhotsk Ocean; Wunugetu

1. Introduction

The Central Asian Orogenic Belt (CAOB), located between the Siberian Craton and the North China Craton, is recognized as one of the largest Phanerozoic orogenic belts globally. Its extensive geological history features the accretion of continental crust induced by oceanic subduction, the convergence of multiple plates, intracontinental orogeny, and associated multistage tectono-magmatic activity. Hence, the deep magmatic activity and

mineralization related to the CAOB's formation and evolution have garnered significant interest from geologists worldwide [1–8]. Within the CAOB, multiple world-class porphyry copper deposits, such as Oyu Tolgoi, Erdenet, and Aktogai–Aiderly, have been identified, positioning this region as a premier porphyry copper belt on a global scale, also referred to as the Central Asian Metallogenic Belt [9]. This belt, along with the Circum-Pacific and Tethyan metallogenic belts, constitutes one of the three principal global copper metallogenic provinces [10]. Situated in the eastern segment of the CAOB, Northeast China emerged from the amalgamation of various microblocks, including the Erguna, Xing'an, Songnen-Zhangguangcai Range, Jiamusi, and Xingkai blocks [11], highlighting its importance as a notable copper-bearing region in China.

The Wunugetu deposit, situated in the southern Erguna block of Northeast China (Figure 1a), represents a significant porphyry copper–molybdenum deposit within the eastern CAOB. Since its identification, the deposit has garnered considerable attention from the geological community [12–14]. Extensive studies of this deposit focus on its geological characteristics, the isotopic geochronology and litho-geochemistry of the ore-hosting surrounding rocks, and ore-forming fluids [12,15–17]. However, debates persist regarding the metallogenic periods and geodynamic setting of the Wunugetu deposit. Wang Zhitian's (1988) initial K-Ar dating of monzogranite porphyry stocks within the deposit yielded an age of 138 Ma [12], leading to the hypothesis of a Late Yanshanian origin. Qin Kezhang (1999), through Rb-Sr dating of the ore-hosting monzogranite porphyries and K-Ar dating of altered sericite, proposed that the deposit formed between 180 and 190 Ma, indicating an Early Jurassic age of this copper–molybdenum deposit [15]. Advancements in analytical methods allowed Tan Gang (2010) to determine a formation age of 177 Ma using Re-Os isotopic dating of the molybdenite [17]. These studies demonstrate that the Wunugetu deposit experienced intense magmatic activity and mineralization events during the Early Jurassic. However, there is limited information on Late Triassic and Middle Jurassic intrusions within the deposit. This study delves into the geological, ore-body, and ore characteristics of the Wunugetu deposit. Employing zircon U-Pb dating, Hf isotope analysis, and whole-rock geochemistry of the ore-hosting porphyritic monzogranites and the late-stage intrusive rhyolitic porphyries, this study aims to constrain the formation periods of ore-forming rock masses and identify the genetic types, source traits, and tectonic setting of the rock masses and late-stage dykes. Additionally, the new data can be used to effectively elucidate the geodynamic context of copper–molybdenum mineralization in the Wunugetu deposit.

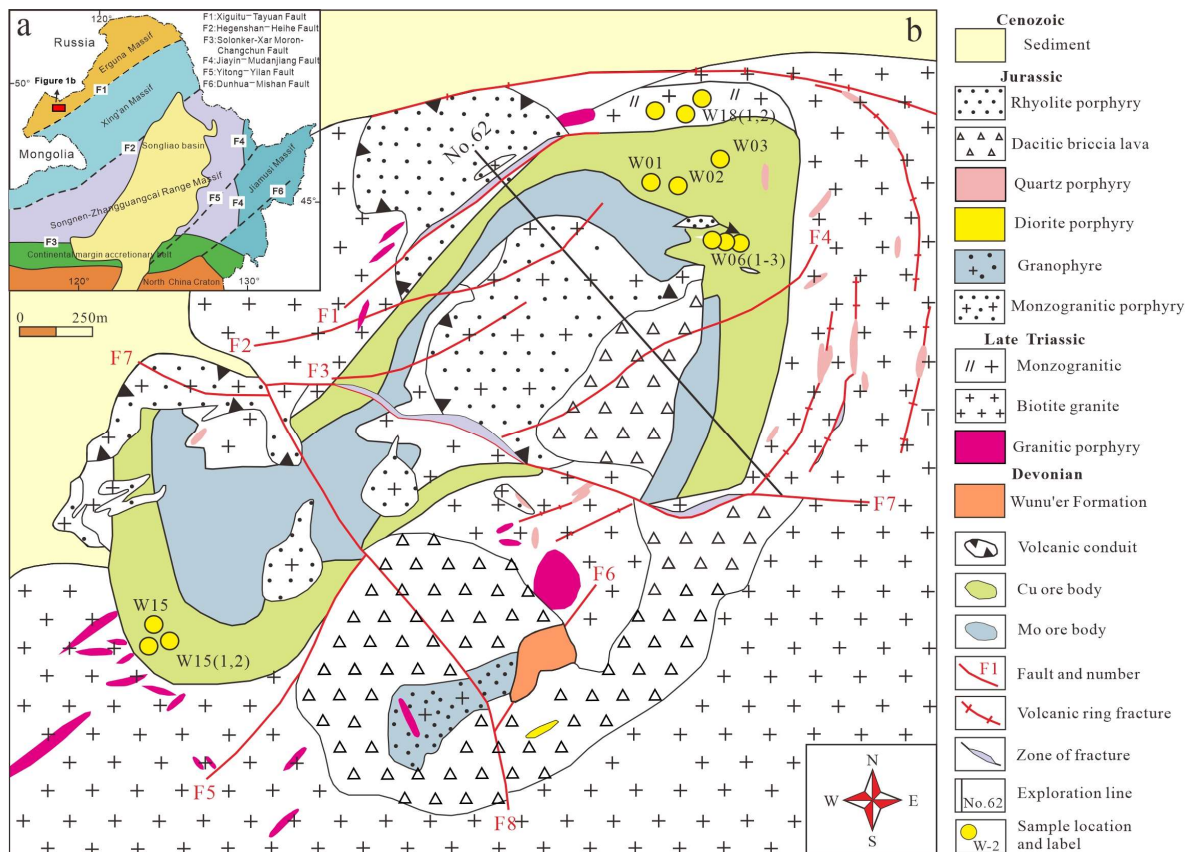


Figure 1. (a) Tectonic location map of the Wunugetu porphyry copper–molybdenum deposit; (b) Geological map of the Wunugetu deposit showing the main lithologies and faults with a volcanic edifice [18].

2. Geological Setting

2.1. Regional Geological Setting

Located about 24 km southwest of Manzhouli City, the Wunugetu deposit is positioned in the central part of the Erguna block, nestled between the Mongol-Okhotsk suture zone (MOSZ) and the Xiguitu-Tayuan fault (Figure 1a). In the Paleozoic era, the Erguna block, influenced by the evolution of the Paleo-Asian Ocean tectonic system, experienced the complex amalgamation of several microblocks within the CAOB [19,20]. From the Late Paleozoic to the Mesozoic, the block fell under the tectonic influence of the Mongol-Okhotsk Ocean tectonic domain [19–23]. The superposition of multiple tectonic domains has endowed this block with highly developed regional fault structures, primarily including a series of E–W- and NE–NNE-trending faults, as well as secondary faults. The oldest exposed strata within the Erguna block consist mainly of Precambrian strata, overlain by Paleozoic and Mesozoic layers. The Precambrian strata are chiefly made up of a crystalline basement composed mainly of schists, leptites, and quartzites from the Neoproterozoic Jiageda Formation (Ptj). The Paleozoic sequence mainly comprises volcanic and terrigenous clastic rocks from the Middle Devonian Wunu'er Formation, while the Mesozoic strata encompass intermediate-mafic volcanic and pyroclastic rocks from the Middle Jurassic Tamulangou Formation, intermediate-acid volcanic rocks from the Shangkuli Formation, and acidic volcanic and pyroclastic rocks from the Upper Jurassic Manketouebo and Manitu formations. The complex process of tectonic evolution has resulted in frequent regional magmatic activity, with Mesozoic granites being the most extensively developed. The region hosts several significant deposits, including the Badaguan copper–molybdenum deposit, the Wunugetu deposit, the Jiawula and Halasheng lead–zinc–silver deposits, and

the Chaganbulagen silver–lead–zinc deposit, all of which are intimately linked to the Mesozoic magmatic activity [15,18,24,25].

2.2. Geological Setting of the Wunugetu Deposit

The Wunugetu deposit was discovered by the No. 706 Team of the Heilongjiang Nonferrous Metal Geological Survey in 1978. By 2006, the deposit had 1.106 million tons of copper and 0.362 million tons of molybdenum identified, establishing it as the most significant large-scale porphyry copper–molybdenum deposit within the Erguna block [13]. In 2008, the China National Gold Group Co., Ltd. (Beijing, China) acquired the Wunugetu deposit to further its exploration and production endeavors.

The exposed strata in the Wunugetu deposit encompass the Devonian Wunu'er Formation's andesites and crystalline limestones (southwest), Upper Jurassic volcanic rocks (north), and extensive Quaternary unconsolidated deposits (Figure 1b).

The Wunugetu deposit underwent two distinct magmatic phases. The first phase, during the Late Triassic, produced biotite granites, monzogranites, and granite porphyries, which together cover about 60% of the deposit's total area. The biotite granites and monzogranites, forming batholiths, extend across the deposit and its vicinity, covering an exposed area of approximately 110 km². These rocks are crucial as the ore-hosting rock masses and surrounding rocks of the deposit.

The second magmatic phase, in the Early Jurassic, led to the formation of a volcanic edifice. The volcanic rocks mainly consist of andesitic agglomerates, while the lithologic assemblages of intrusions primarily comprise monzogranite porphyries, quartz porphyries, diorite porphyrites, and rhyolitic porphyries. The rhyolitic porphyries, intruding into the mineral-bearing monzogranite porphyries, show no signs of mineralization or alteration zones. The monzogranite porphyries are distributed in the central portion of the deposit. They are disrupted by the late-stage F7 fault, making them a key ore-hosting rock mass. Additionally, the outcrops in the deposit include minor quantities of dacitic breccias, quartz porphyries, and diorite porphyrites.

Fault structures are prominent in the Wunugetu deposit, including NE-, NNW-, and nearly E–W-trending faults, along with ring-shaped faults in volcanic areas. The NE-trending and ring-shaped faults developed during the mineralization period, whereas the NW-oriented F8 fault emerged in the later stages of mineralization. These faults cut through ore bodies, disrupting their continuity. The E–W-trending F7 fault divides the ore bodies into southern and northern segments.

3. Ore Body Characteristics

The ore bodies within the Wunugetu deposit are arranged in a ring-like pattern orienting NWE, with monzogranite porphyries at their core. The area of mineralization spans roughly 2600 m in length and about 1400 m in width. These ore bodies have a strike of 50° and a dip direction of WN. The F7 fault causes a horizontal displacement of approximately 700 m, thereby splitting the ore bodies into two distinct segments: the southern segment spans about 800 m in width, while the northern segment extends approximately 900 m across. Both segments are subjected to hydrothermal alteration within the deposit. The Wunugetu deposit exhibits typical alteration zones of porphyry-type mineralization, covering an area of approximately 5 km². These zones roughly comprise potassic (Or), quartz-sericite (Qs), and illite-hydromica (IH) alteration zones [15]. The primary alterations observed include silicification, potassic feldspathization, sericitization, illitization, muscovitization, carbonatization, and kaolinization, with chloritization and epidotization being relatively less common (Figure 2).

The potassic zone (Or), centrally located within the deposit, is found predominantly in the monzogranite porphyry rock masses. The alteration minerals characteristic of this zone are mainly K-feldspar and biotite, with sericite present in smaller quantities (Figure 2a). Molybdenite is the principal type of mineralization in this zone, along with notable occurrences of chalcopyrite and pyrite mineralizations.

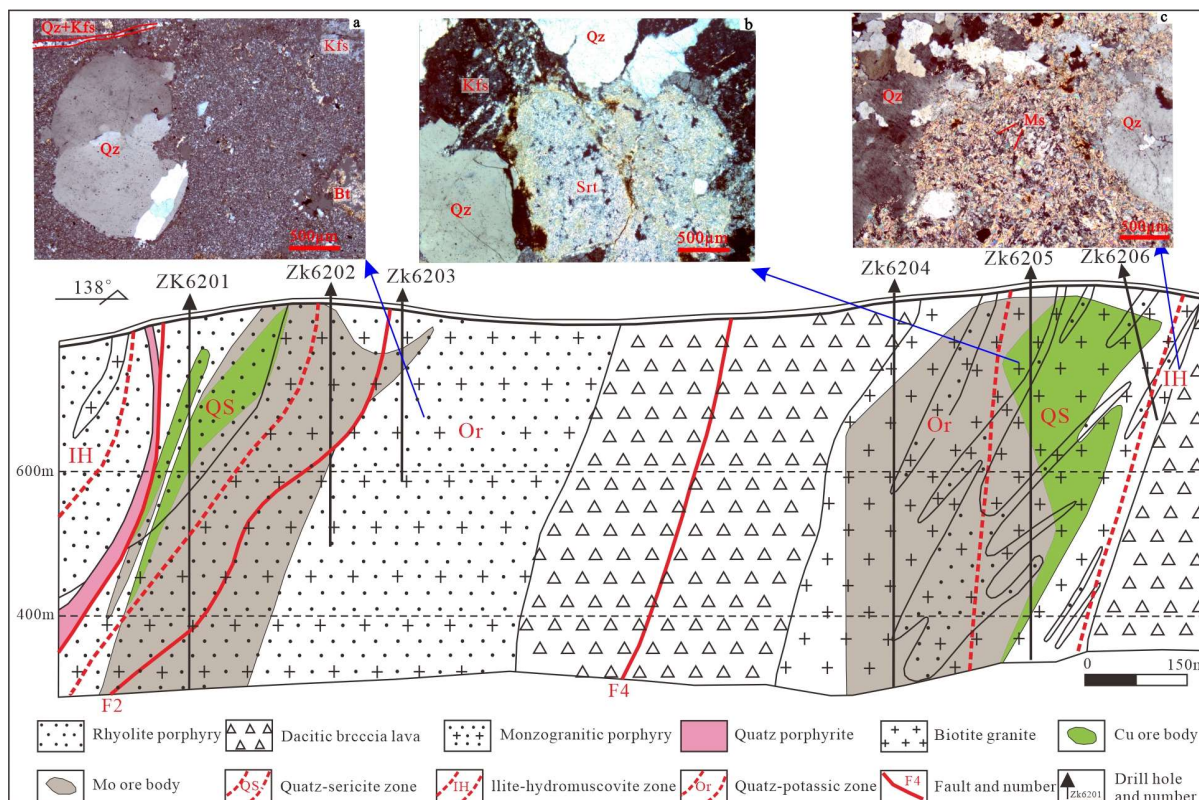


Figure 2. Northwest–southeast section (620 line) through the Wunugetu deposit showing the relationship of host monzogranitic porphyry, alteration, and mineralization [24]. Micrographs of potassium feldspathization (a), quartz-sericitization (b), and illite-hydromica (c). Bt—biotite, Qz—quartz, Pl—plagioclase, Kfs—feldspar, Srt—sericite, Ms—Muscovite.

The quartz-sericite zone (Qs) extends through the biotite granites and their contact zone with the monzogranite porphyries. This zone is rich in alteration minerals such as quartz, sericite (Figure 2b), and carbonate. The ore minerals in this zone include molybdenite, chalcopyrite, malachite, pyrite, and azurite.

The illite-hydromica zone (IH), located within biotite granites on the periphery of the deposit and rhyolites in the northern part, features alteration minerals like illite, hydromuscovite (Figure 2c), carbonate, and kaolinite. This zone also exhibits lead and zinc mineralizations.

4. Sampling and Methodology

4.1. Sampling and Lithofacies Characteristics of Samples

A total of 14 samples were gathered, comprising three monzogranite samples (WNG01, WNG02, and WNG03), four rhyolitic porphyry samples (WNG06, WNG06-1, WNG06-2, and WNG06-3; Figure 3a) from the deposit’s northern area, four monzogranite samples (WNG15-1, WNG15-2, WNG15-3, and WNG15; Figure 3b) from the southern portion, and three additional monzogranite samples (WNG18-1, WNG18-2, and WNG18-3) from the deposit’s periphery. The specific sampling locations are depicted in Figure 1b.

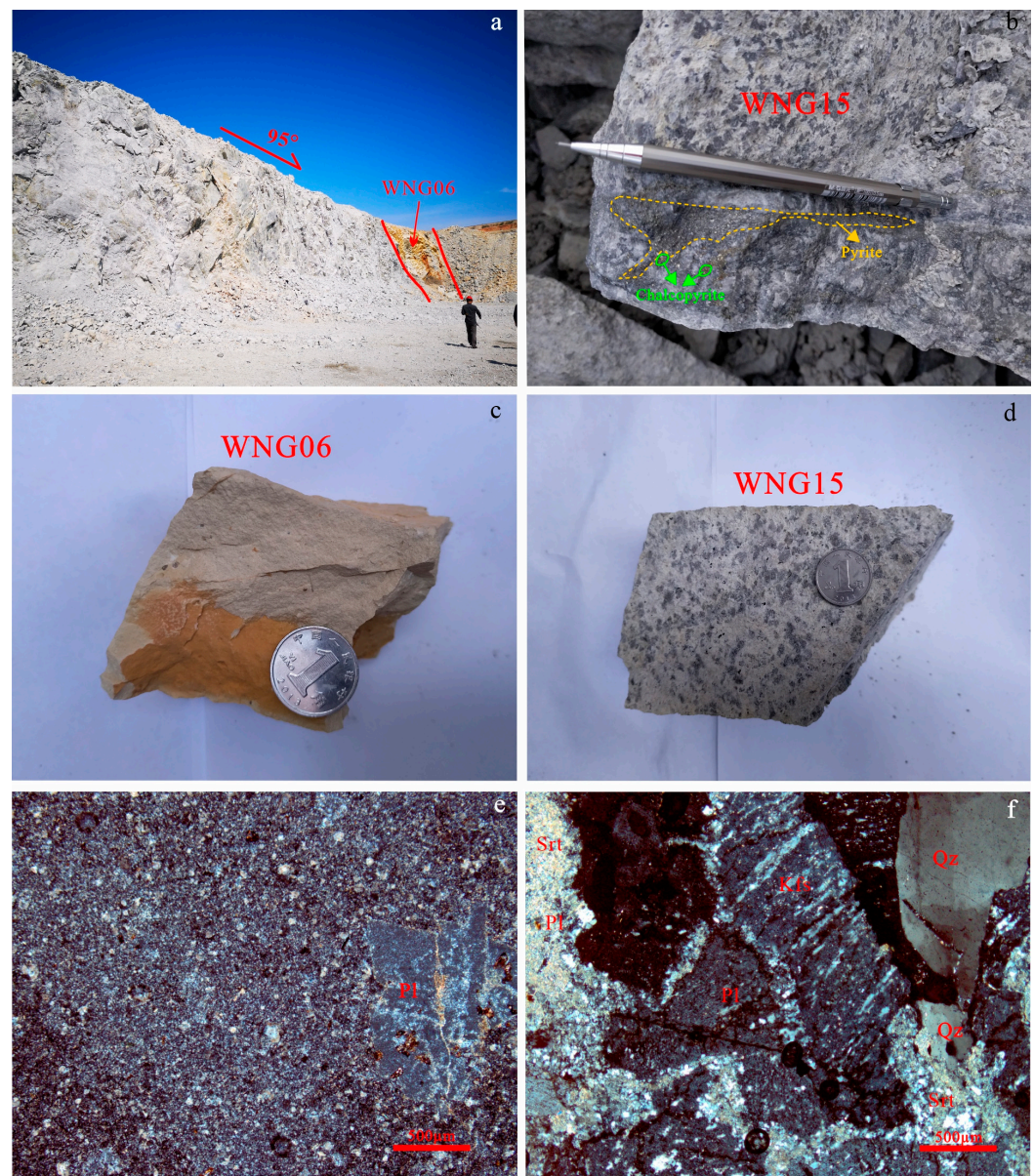


Figure 3. Field outcrops, hand specimens, and microscopic photos of the monzogranites and rhyolitic porphyries in the Wunugetu deposit. Qz—quartz, Pl—plagioclase, Kfs—feldspar, Srt—sericite. (a) Field outcrops and sampling locations of rhyolitic porphyries; (b) Sampling location of monzogranite, with fine veins of pyrite and chalcopyrite; (c) Monzogranite hand specimens; (d) Rhyolitic porphyry hand specimen; (e) Microscopic photos of rhyolitic porphyry; (f) Microscopic photos of monzogranites.

4.2. Zircon U-Pb Dating

Zircon monomineralic separation, target preparation, cathodoluminescence (CL) imaging, and zircon U-Pb dating were performed at the laboratory of Yandu Zhongshi Testing Technology Co., Ltd. (Beijing, China) The procedures utilized a New Wave UP213 laser ablation system and an M90 inductively coupled plasma mass spectrometer (ICP-MS) manufactured by Analytik Jena AG. Zircon reference materials 91500 and Plesovice employed exhibited the values recommended [26,27], as calculated using ZSkit software ver. 1.1.0. The quantification of trace elements in zircon utilized SRM610 and Si as the external and internal standards, respectively [28]. For U-Pb isotopic dating, zircon reference material 91500 was used as an external standard for isotopic fractionation correction. The U-Pb age concordia diagrams and the weighted average ages of the zircon samples were generated

using Isoplot/Exver3 [29]. Additionally, the correction of common lead in U-Pb analyses was performed following Andersen's (2002) method [30].

4.3. In-Situ Lu-Hf Isotopes of Zircon

In-situ zircon Lu-Hf isotopic analyses were performed utilizing a Neptune Plus MC-ICP-MS manufactured by Thermo-Fisher and a New Wave UP213 laser ablation system, with the procedures and calibration methods akin to those proposed by Wu Fuyuan et al. (2007) [31]. Laser ablation was executed for 31 s at a frequency of 8 Hz and an energy density of 16 J/cm². Considering the exceptionally low ¹⁷⁶Lu/¹⁷⁷Hf ratios in zircon, typically below 0.002, the isotopic interference of ¹⁷⁶Lu on ¹⁷⁶Hf was deemed negligible. The isotopic fractionation factor of Yb was calculated using the average ¹⁷³Yb/¹⁷²Yb ratios of various test points, followed by removal of the isobaric interference of ¹⁷⁶Yb on ¹⁷⁶Hf. The ¹⁷³Yb/¹⁷²Yb ratio was established at 1.35274.

4.4. Whole-Rock Major- and Trace-Element Analyses

Complete silicate analysis was performed at the laboratory of Yandu Zhongshi Testing Technology Co., Ltd. Major element analysis utilized the acid dissolution method in conjunction with a Zetium X-ray fluorescence spectrometer (XRF) from PANalytical, with analytical precision errors under 0.1%. Trace element analysis was carried out with an M90 ICP-MS from Analytik Jena AG, with analytical errors maintained below 10%.

5. Results

5.1. Petrography

The rhyolitic porphyries, as stocks, intrude into granite porphyries, characterized by porphyritic textures and blocky structures. Their phenocrysts, making up 10% of the composition, consist of quartz (5%) and feldspar (5%), with particle sizes between 0.4 and 1.4 mm. Their matrix, constituting 90%, is mainly feldspar and quartz. It manifests felsitic textures, with radial or fan-shaped grains scattering locally (Figure 3c,e).

The monzogranites comprise plagioclase (35%), alkali feldspar (30%), and quartz (35%), with consistent mineral grain sizes ranging from 1.6 to 3.0 mm. The plagioclase is hypidiomorphic, tabular, and granular, featuring sericite alterations on their surfaces. In contrast, the alkali feldspar appears as xenomorphic grains (Figure 3d,f).

The monzogranite porphyries are composed of plagioclase (30%), alkali feldspar (30%), quartz (32%) (Figure 3d), sericite (5%), and pyrite (3%). The grains are uniform in size, ranging from 1.6 to 3.0 mm. The plagioclase is subhedral, appearing in tabular and granular shapes, with sericite pseudomorphing its surfaces. The alkali feldspar occurs as xenomorphic grains, comprising perthitic feldspar with irregularly vein-like, spotted, and patchy patterns. It exhibits weak sericitization on surfaces, with sericite replacing along the perthite (Figure 3f). The pyrite occurs mainly as euhedral to anhedral grains distributed among the minerals' intergranular spaces.

5.2. Zircon U-Pb Ages

The LA-ICP-MS zircon U-Pb dating data are shown in Table 1, partial zircon CL images are illustrated in Figure 4a,b, and the concordia diagrams with weighted average age curves are presented in Figure 5a,b. Zircon grains from rhyolitic porphyry sample WNG06 ranged from idiomorphic to hypidiomorphic columnar shapes, with sizes ranging from 50 to 150 μm. These grains were primarily short columnar, followed by long columnar, with length/width ratios from 1:1 to 2.5:1 and minor fissures occasionally visible. Oscillatory zoning was observed in the CL images of these zircon grains. Their Th/U ratios spanned from 0.74 to 1.34, all above 0.1, indicating a magmatic origin for these grains. Analysis of 22 test points on this sample yielded ²⁰⁶Pb/²³⁸U ages between 169 and 173 Ma, corresponding to weighted average ages of 170.49 ± 0.81 Ma (MSWD = 0.68).

Table 1. LA-ICP-MS zircon U-Pb dating data of Wunugetu rhyolite porphyry and monzogranites.

Test Point Number	Th ($\times 10^{-6}$)	U ($\times 10^{-6}$)	Th/U	Isotope Atomic Ratio						Isotopic Age (Ma)									
				$^{207}\text{Pb}/^{206}\text{Pb}$	1 σ	$^{207}\text{Pb}/^{235}\text{U}$	1 σ	$^{206}\text{Pb}/^{238}\text{U}$	1 σ	$^{208}\text{Pb}/^{232}\text{Th}$	1 σ	$^{207}\text{Pb}/^{206}\text{Pb}$	1 σ	$^{207}\text{Pb}/^{235}\text{U}$	1 σ	$^{206}\text{Pb}/^{238}\text{U}$	1 σ	$^{208}\text{Pb}/^{232}\text{Th}$	1 σ
Sample WNG06																			
WNG06-08	801	724	1.11	0.05012	0.00097	0.18207	0.00359	0.02636	0.00023	0.00812	0.00013	200	45	170	3	168	1	163	3
WNG06-26	1007	932	1.08	0.04959	0.00107	0.18035	0.00413	0.02638	0.00029	0.00808	0.00022	176	51	168	4	168	2	163	4
WNG06-21	516	618	0.83	0.05038	0.00126	0.18452	0.00511	0.02653	0.00036	0.00852	0.00038	213	58	172	4	169	2	171	8
WNG06-23	614	689	0.89	0.04959	0.00120	0.18107	0.00453	0.02654	0.00032	0.00795	0.00031	176	57	169	4	169	2	160	6
WNG06-13	722	783	0.92	0.04972	0.00148	0.18326	0.00615	0.02663	0.00035	0.00826	0.00024	182	69	171	5	169	2	166	5
WNG06-20	997	821	1.22	0.05074	0.00137	0.18636	0.00469	0.02664	0.00030	0.00824	0.00038	229	62	174	4	169	2	166	8
WNG06-30	630	692	0.91	0.04925	0.00095	0.18037	0.00333	0.02665	0.00032	0.00867	0.00028	160	45	168	3	170	2	175	6
WNG06-01	607	624	0.97	0.05027	0.00117	0.18590	0.00398	0.02678	0.00026	0.00855	0.00018	208	54	173	3	170	2	172	4
WNG06-22	475	602	0.79	0.04981	0.00140	0.18458	0.00591	0.02679	0.00040	0.00874	0.00042	186	65	172	5	170	3	176	8
WNG06-25	715	727	0.98	0.04887	0.00110	0.18015	0.00403	0.02680	0.00032	0.00860	0.00031	142	53	168	3	170	2	173	6
WNG06-27	826	823	1.00	0.04911	0.00100	0.18165	0.00409	0.02682	0.00031	0.00813	0.00020	153	48	169	4	171	2	164	4
WNG06-16	561	598	0.94	0.05070	0.00120	0.18792	0.00463	0.02682	0.00026	0.00861	0.00026	227	55	175	4	171	2	173	5
WNG06-14	457	570	0.80	0.04917	0.00155	0.18074	0.00574	0.02682	0.00033	0.00859	0.00026	156	74	169	5	171	2	173	5
WNG06-15	502	570	0.88	0.05059	0.00132	0.18667	0.00475	0.02683	0.00033	0.00805	0.00025	222	61	174	4	171	2	162	5
WNG06-09	341	458	0.74	0.05001	0.00172	0.18565	0.00656	0.02686	0.00034	0.00831	0.00021	195	80	173	6	171	2	167	4
WNG06-29	664	701	0.95	0.04942	0.00124	0.18396	0.00511	0.02702	0.00045	0.00880	0.00026	168	59	171	4	172	3	177	5
WNG06-03	589	651	0.90	0.05033	0.00105	0.18768	0.00423	0.02706	0.00029	0.00889	0.00015	210	48	175	4	172	2	179	3
WNG06-05	865	748	1.16	0.05059	0.00094	0.18864	0.00365	0.02708	0.00029	0.00868	0.00013	222	43	175	3	172	2	175	3
WNG06-28	304	411	0.74	0.04884	0.00155	0.18165	0.00558	0.02709	0.00035	0.00857	0.00026	140	74	169	5	172	2	172	5
WNG06-10	789	765	1.03	0.05071	0.00114	0.18990	0.00419	0.02712	0.00025	0.00902	0.00027	228	52	177	4	172	2	181	5
WNG06-02	2099	1566	1.34	0.04953	0.00118	0.18585	0.00464	0.02717	0.00031	0.00864	0.00013	173	56	173	4	173	2	174	3
WNG06-12	804	740	1.09	0.04900	0.00158	0.18321	0.00601	0.02720	0.00040	0.00917	0.00033	148	76	171	5	173	3	184	7
Sample WNG15																			
WNG15-10	667	959	0.63	0.05252	0.00294	0.23892	0.01295	0.03299	0.00046	0.01035	0.00012	308	131	218	11	209	3	208	2
WNG15-27	1137	2309	0.47	0.05220	0.00287	0.23680	0.01276	0.03290	0.00035	0.01033	0.00010	294	128	216	10	209	2	208	2
WNG15-04	569	1121	0.48	0.05198	0.00200	0.23667	0.00878	0.03302	0.00033	0.01037	0.00009	285	90	216	7	209	2	209	2
WNG15-11	91	236	0.36	0.05154	0.00135	0.23341	0.00653	0.03280	0.00043	0.01136	0.00035	265	40	213	5	208	3	228	7
WNG15-18	201	423	0.45	0.05138	0.00148	0.22978	0.00675	0.03239	0.00040	0.01002	0.00035	258	45	210	6	205	2	202	7
WNG15-19	313	586	0.49	0.05129	0.00157	0.23114	0.00799	0.03256	0.00052	0.00972	0.00041	254	50	211	7	207	3	196	8
WNG15-30	209	462	0.42	0.05112	0.00090	0.23118	0.00456	0.03284	0.00034	0.01027	0.00023	246	27	211	4	208	2	207	5
WNG15-29	565	1261	0.43	0.05090	0.00075	0.23156	0.00421	0.03290	0.00030	0.01024	0.00026	236	25	211	3	209	2	206	5
WNG15-08	1453	2266	0.60	0.05084	0.00073	0.23251	0.00365	0.03308	0.00041	0.01070	0.00029	233	17	212	3	210	3	215	6
WNG15-14	233	259	0.85	0.05074	0.00144	0.22922	0.00690	0.03277	0.00040	0.01044	0.00021	229	47	210	6	208	2	210	4
WNG15-17	274	544	0.46	0.05076	0.00113	0.23267	0.00560	0.03316	0.00039	0.01080	0.00038	230	34	212	5	210	2	217	8
WNG15-28	1611	2523	0.60	0.05057	0.00087	0.23200	0.00487	0.03311	0.00043	0.01046	0.00046	221	26	212	4	210	3	210	9
WNG15-05	250	641	0.37	0.05054	0.00092	0.23153	0.00511	0.03309	0.00032	0.01065	0.00041	220	33	211	4	210	2	214	8
WNG15-12	443	1048	0.39	0.05050	0.00137	0.23097	0.00583	0.03313	0.00038	0.01092	0.00037	218	37	211	5	210	2	220	7
WNG15-24	425	1234	0.32	0.05048	0.00114	0.23252	0.00509	0.03332	0.00039	0.01015	0.00047	217	30	212	4	211	2	204	9
WNG15-16	1041	1784	0.56	0.05028	0.00068	0.22845	0.00376	0.03288	0.00032	0.01002	0.00031	208	21	209	3	209	2	202	6
WNG15-09	2274	2216	0.97	0.04959	0.00399	0.22341	0.01758	0.03267	0.00055	0.01032	0.00015	176	183	205	15	207	3	208	3
WNG15-06	339	481	0.67	0.04950	0.00086	0.22857	0.00460	0.03340	0.00027	0.01013	0.00027	171	32	209	4	212	2	204	5

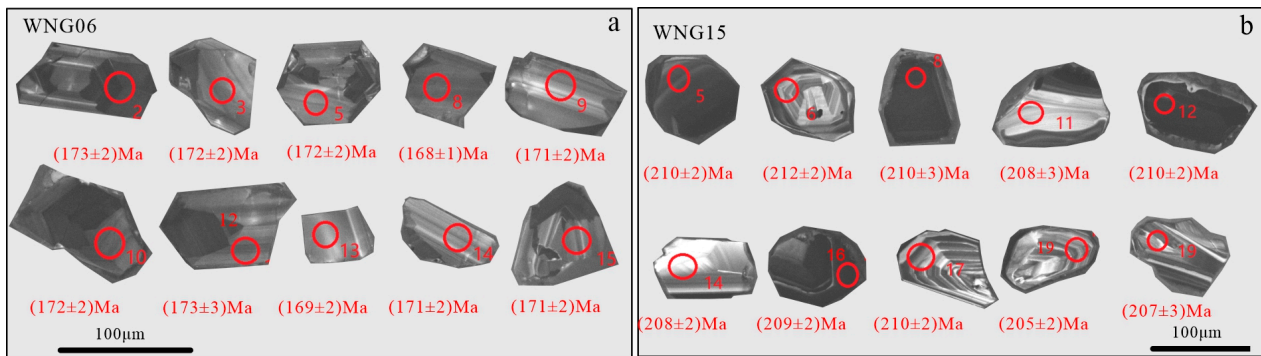


Figure 4. Cathodoluminescence images of zircons in the Wunugetu deposit. (a) Rhyolite Porphyry; (b) Monzogranite.

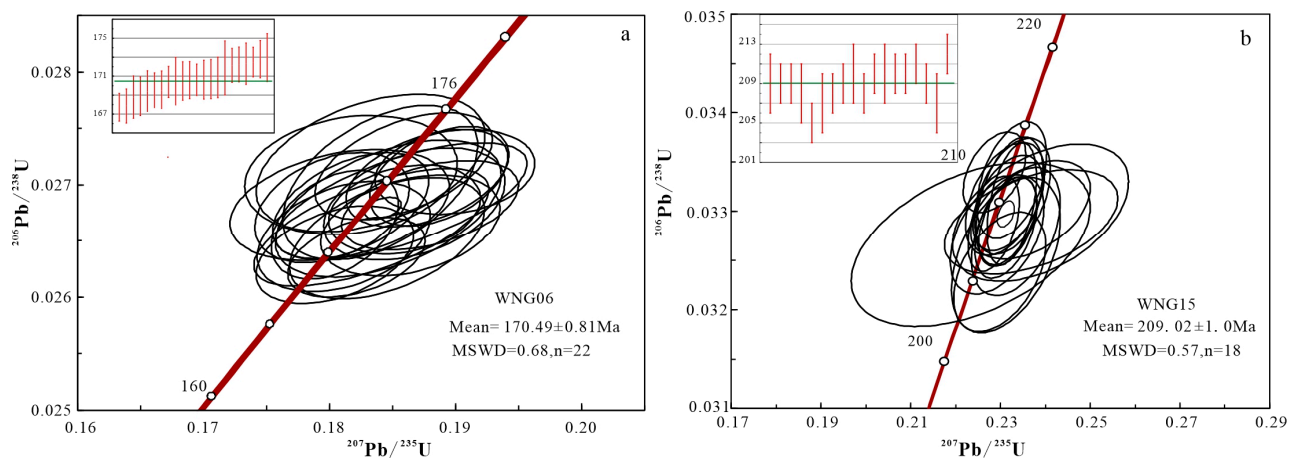


Figure 5. Zircon LA-ICP-MS U-Pb concordia diagrams from Wunugetu copper-gold deposit. (a) Rhyolitic porphyries; (b) Monzogranite.

Zircon grains from monzogranite sample WNG15 displayed shapes from idiomorphic to hypidiomorphic columnar, with sizes varying between 50 to 200 µm. These grains were predominantly short columnar and secondarily long columnar, with length/width ratios ranging between 1:1 and 3:1. Oscillatory zoning was apparent in the CL images of the zircon grains. The Th/U ratios of the zircons spanned from 0.32 to 0.97, all above the 0.1 threshold, indicating a magmatic origin. Analysis of 18 test points on this sample revealed $^{206}\text{Pb}/^{238}\text{U}$ ages between 205 to 218 Ma, with weighted average ages of 209.02 ± 1.0 Ma (MSWD = 0.57).

5.3. In-Situ Lu-Hf Isotopes of Zircon

The in-situ Lu-Hf isotopic analysis results of zircon are summarized in Table 2. The Hf isotopic data were calculated using U-Pb ages obtained from the same zircon test points. Zircon grains from samples WNG06 and WNG15 exhibited $^{176}\text{Hf}/^{177}\text{Hf}$ ratios within the ranges of 0.282742–0.282874 and 0.282658–0.282784, respectively, corresponding to $\epsilon\text{Hf}(t)$ values ranging from +2.4 to +10.8 for WNG06 and from +0.3 to +4.6 for WNG15. The derived two-stage model ages ($T_{\text{DM}2}$) for these samples were between 727 to 1058 Ma for WNG06 and 949 to 1227 Ma for WNG15.

Table 2. Zircon Hf isotope analysis results of Wunugetu rhyolite porphyry and monzogranites.

Sample	Age (Ma)	¹⁷⁶ Yb/ ¹⁷⁷ Hf	2σ	¹⁷⁶ Lu/ ¹⁷⁷ Hf	2σ	¹⁷⁶ Hf/ ¹⁷⁷ Hf	2σ	ε _{Hf} (0)	ε _{Hf} (t)	T _{DM1} (Ma)	T _{DM2} (Ma)	f _{Lu/Hf}
WNG06-002	173	0.092751	0.000975	0.002781	0.000029	0.282836	0.000023	2.3	5.7	620	850	−0.92
WNG06-003	172	0.097305	0.001427	0.002702	0.000047	0.282847	0.000025	2.7	6.1	601	823	−0.92
WNG06-005	172	0.084428	0.000322	0.002441	0.000032	0.282742	0.000026	−1.1	2.4	751	1058	−0.93
WNG06-008	168	0.087212	0.001147	0.002416	0.000046	0.282782	0.000021	0.4	3.8	691	970	−0.93
WNG06-009	171	0.081093	0.001396	0.002398	0.000048	0.282865	0.000025	3.3	6.8	569	781	−0.93
WNG06-010	172	0.073125	0.000371	0.002032	0.000028	0.282855	0.000020	3.0	6.5	578	800	−0.94
WNG06-012	173	0.099545	0.000903	0.002832	0.000046	0.282858	0.000027	3.0	6.5	587	800	−0.91
WNG06-013	169	0.093224	0.000430	0.002751	0.000027	0.282788	0.000027	0.6	4.0	690	959	−0.92
WNG06-014	171	0.077629	0.000628	0.002241	0.000018	0.282889	0.000027	4.1	7.6	532	727	−0.93
WNG06-015	171	0.083756	0.000953	0.002540	0.000047	0.282874	0.000028	3.6	7.1	558	762	−0.92
WNG15-005	210	0.062887	0.001353	0.002038	0.000049	0.282684	0.000023	−3.1	1.2	828	1166	−0.94
WNG15-006	212	0.081818	0.002085	0.002546	0.000050	0.282658	0.000020	−4.0	0.3	877	1227	−0.92
WNG15-008	210	0.110316	0.000582	0.003513	0.000064	0.282673	0.000028	−3.5	0.6	878	1202	−0.89
WNG15-011	208	0.047510	0.003141	0.001509	0.000117	0.282732	0.000023	−1.4	3.0	746	1053	−0.95
WNG15-012	210	0.097143	0.001717	0.003026	0.000081	0.282774	0.000022	0.1	4.3	716	972	−0.91
WNG15-014	208	0.092412	0.002386	0.002985	0.000046	0.282784	0.000020	0.4	4.6	700	949	−0.91
WNG15-016	209	0.064028	0.001103	0.001971	0.000037	0.282751	0.000016	−0.7	3.6	729	1015	−0.94
WNG15-017	210	0.085413	0.000815	0.002533	0.000018	0.282736	0.000019	−1.3	3.0	762	1052	−0.92
WNG15-018	205	0.076844	0.000813	0.002362	0.000023	0.282747	0.000015	−0.9	3.3	742	1028	−0.93
WNG15-019	207	0.070343	0.000818	0.002212	0.000025	0.282740	0.000019	−1.1	3.1	750	1043	−0.93

5.4. Whole-Rock Major and Trace Element Analyses

The analytical outcomes for major, trace, and rare earth elements (REEs) across 12 rock samples are compiled in Table 3. Regarding major elements, these samples contained 70.16–80.47 wt.% SiO₂, 10.98–14.37 wt.% Al₂O₃ (rhyolite), 0.17–3.77 wt.% Na₂O, 2.95–9.36 wt.% K₂O, 0.06–0.99 wt.% CaO, 0.14–0.37 wt.% MgO, and 3.42–10.10 wt.% Na₂O + K₂O, indicating high silicon content and depletion of sodium generally. The total alkali-silica (TAS) diagram shows that most samples fell within the granite field (Figure 6), in line with petrographic results.

Table 3. Analysis results of major elements (wt.%), rare earth elements, and trace elements (ppm) in Wunugetu rhyolite porphyry and monzogranites.

No.3	W06-1	W06-2	W06-3	W01	W02	W03	W15-1	W15-2	W15-3	W18-1	W18-2	W18-3
Rock Type	Porphyry Rhyolite						Monzogranites					
Major element (wt.%)												
SiO ₂	76.35	75.77	77.45	73.44	73.16	80.47	75.36	76.69	77.71	74.40	75.13	74.92
Al ₂ O ₃	12.86	12.87	12.72	14.25	14.37	11.38	13.01	12.89	10.98	13.52	13.24	12.81
Na ₂ O	0.23	0.23	0.23	0.74	0.74	0.17	0.22	0.30	1.59	3.77	3.55	3.73
K ₂ O	5.91	5.33	5.00	9.36	8.24	3.25	5.05	7.15	5.09	3.94	4.14	2.95
CaO	0.09	0.12	0.09	0.07	0.11	0.06	0.06	0.07	0.15	0.99	0.93	0.57
P ₂ O ₅	0.04	0.04	0.04	0.09	0.08	0.05	0.05	0.06	0.05	0.09	0.08	0.07
TiO ₂	0.05	0.05	0.05	0.17	0.17	0.07	0.10	0.09	0.16	0.21	0.18	0.22
MgO	0.17	0.18	0.17	0.17	0.26	0.34	0.34	0.14	0.37	0.27	0.25	0.23
MnO	0.19	0.28	0.11	0.03	0.02	0.03	0.04	0.03	0.04	0.04	0.04	0.03
TFe ₂ O ₃	1.29	1.93	1.03	0.54	0.84	1.44	2.29	0.51	1.34	1.43	1.32	2.89
LOI	2.34	2.82	2.49	0.77	1.38	2.11	2.89	1.46	1.91	0.73	0.74	1.39
TOTAL	99.51	99.63	99.38	99.63	99.36	99.37	99.40	99.38	99.38	99.39	99.58	99.81
Trace element (ppm)												
Rb	62.98	121.78	113.08	117.95	113.48	77.48	146.83	138.72	171.18	158.50	166.50	122.31
Ba	203.79	225.28	839.21	757.42	606.85	303.08	696.06	1041.38	1112.03	604.78	551.03	916.73
Th	2.77	6.09	5.93	15.38	20.62	13.02	19.03	23.97	11.00	13.17	10.23	20.39
U	0.25	0.80	0.58	2.49	2.38	14.72	4.12	7.38	1.62	2.70	2.84	3.21
Ta	0.27	0.51	0.51	1.93	1.88	2.31	1.65	1.00	0.76	1.29	1.08	0.82
Nb	4.05	8.34	7.92	19.01	17.78	13.71	14.18	13.20	12.22	18.78	14.98	12.12
Sr	23.30	50.70	68.98	130.77	109.44	7.36	28.35	80.05	126.96	167.97	157.60	214.75
Zr	24.93	56.69	53.11	109.40	92.35	81.56	95.83	148.81	162.38	89.83	114.23	201.24

Table 3. Cont.

No.3	W06-1	W06-2	W06-3	W01	W02	W03	W15-1	W15-2	W15-3	W18-1	W18-2	W18-3
Rock Type	Porphyry Rhyolite						Monzogranites					
Hf	1.33	2.56	2.48	4.19	3.50	3.63	3.88	4.74	4.59	3.38	3.93	5.30
La	7.21	15.25	16.25	23.06	32.07	29.87	36.42	46.27	37.12	10.74	10.88	54.28
Ce	15.21	32.38	34.44	46.74	64.09	60.42	69.61	82.46	70.73	20.56	20.21	74.95
Pr	1.77	4.10	4.44	5.47	7.29	6.92	8.00	9.15	8.63	2.93	3.28	7.93
Nd	5.76	13.86	15.31	17.99	23.33	22.66	26.14	32.66	32.29	10.51	11.63	23.94
Sm	0.99	2.39	2.63	3.47	4.18	3.91	4.13	5.19	5.83	2.65	2.87	3.26
Eu	0.18	0.41	0.56	0.65	0.67	0.74	0.74	0.94	1.12	0.57	0.57	0.78
Gd	0.78	1.95	1.99	3.56	4.66	4.10	4.04	5.07	5.53	2.98	2.81	3.09
Tb	0.10	0.24	0.21	0.59	0.79	0.70	0.56	0.66	0.83	0.53	0.48	0.35
Dy	0.46	1.16	0.92	3.68	5.03	4.54	3.01	3.62	4.79	3.52	2.95	1.74
Ho	0.09	0.23	0.19	0.80	1.15	1.03	0.65	0.77	0.97	0.80	0.64	0.39
Er	0.28	0.69	0.58	2.54	3.59	3.30	1.99	2.46	2.98	2.52	2.02	1.30
Tm	0.04	0.10	0.08	0.43	0.60	0.59	0.35	0.41	0.50	0.45	0.36	0.22
Yb	0.17	0.51	0.40	2.77	4.30	4.33	2.41	2.75	3.30	2.89	2.46	1.56
Lu	0.04	0.10	0.09	0.49	0.63	0.67	0.42	0.49	0.53	0.49	0.41	0.28
Y	2.50	6.25	5.12	21.35	30.48	29.67	18.14	21.48	26.15	22.18	17.81	10.26
ΣREE	33.08	73.38	78.07	112.24	152.37	143.79	158.48	192.91	175.14	62.13	61.57	174.06
LREE	31.13	68.39	73.63	97.39	131.62	124.53	145.03	176.67	155.71	47.96	49.44	165.14
HREE	1.95	4.99	4.44	14.85	20.76	19.27	13.45	16.24	19.43	14.16	12.13	8.92
LREE/HREE	15.96	13.70	16.59	6.56	6.34	6.46	10.78	10.88	8.01	3.39	4.08	18.51
La _N /Yb _N	31.23	21.48	29.37	5.97	5.35	4.95	10.82	12.07	8.07	2.67	3.17	25.01
δEu	0.64	0.58	0.75	0.57	0.46	0.57	0.55	0.56	0.60	0.62	0.62	0.75
δCe	1.05	1.00	0.99	1.02	1.03	1.03	1.00	0.98	0.97	0.90	0.83	0.89

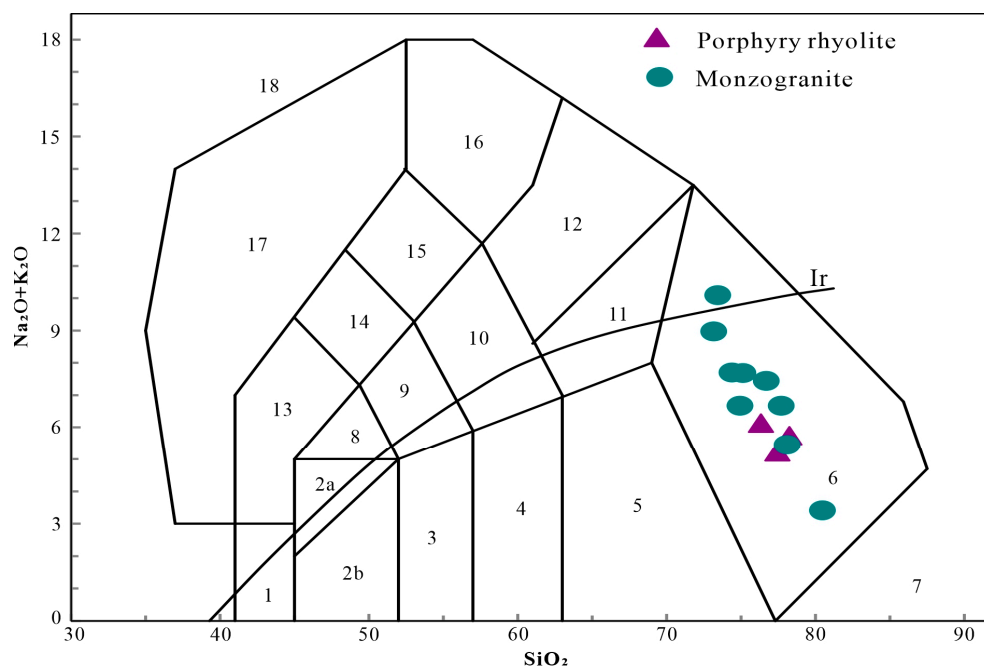


Figure 6. TAS discrimination diagram of igneous rocks in the Wunugetu deposit. Ir—Irvine boundary [32]; above is alkaline, below is subalkaline. 1—Peridotgabbro; 2a—Alkali Gabbro; 2b—Subalkaline Gabbro; 3—Gabbroic Diorite; 4—Diorite; 5—Granodiorite; 6—Granite; 7—Quartzolite; 8—Monzogabbro; 9—Monzodiorite; 10—Monzosyenite; 11—Quartz Monzonite; 12—Syenite; 13—Foid Gabbro; 14—Foid Monzodiorite; 15—Foid Monzosyenite; 16—Foidolite Syenite; 17—Foidolite; 18—Tawite/Urtite/Italite.

Regarding major elements, the monzogranite samples contained 73.16–80.47 wt.% SiO₂, 10.98–14.37 wt.% Al₂O₃, 0.17–3.77 wt.% Na₂O, and 2.95–9.36 wt.% K₂O. Notably,

samples WNG01, WNG02, and WNG15-2 exhibited elevated K_2O levels, suggesting the potential influence of potassic feldsparization within the deposit. The CaO varied from 0.06 to 0.99 wt.%, MgO from 0.14 to 0.37 wt.%, and total alkalis ($Na_2O + K_2O$) from 3.42 to 10.10 wt.%, indicating high silica and low sodium. All the samples fell within the granite field on the TAS diagram (Figure 6).

The rhyolitic porphyry samples revealed SiO_2 between 75.77 wt.% and 77.45 wt.%, Al_2O_3 from 10.98 to 14.37 wt.%, Na_2O at 0.23 wt.%, K_2O from 5.00 to 5.91 wt.%, CaO between 0.09 and 0.12 wt.%, MgO from 0.17 to 0.18 wt.%, and $Na_2O + K_2O$ from 5.23 to 6.14 wt.%, also demonstrating high silica and low sodium traits. These samples fell within the granite field on the TAS diagram (Figure 6).

In the K_2O – SiO_2 diagram (Figure 7a), the samples fell within the high-K calc-alkaline to shoshonitic series zones, with one point in the calc-alkaline series zone, indicating the rhyolite and monzogranite samples' classification belongs to these series. All rock samples, with aluminum saturation index (A/CNK) values from 1.1 to 2.9, fell within the peraluminous zone on the A/NK vs. A/CNK diagram (Figure 7b).

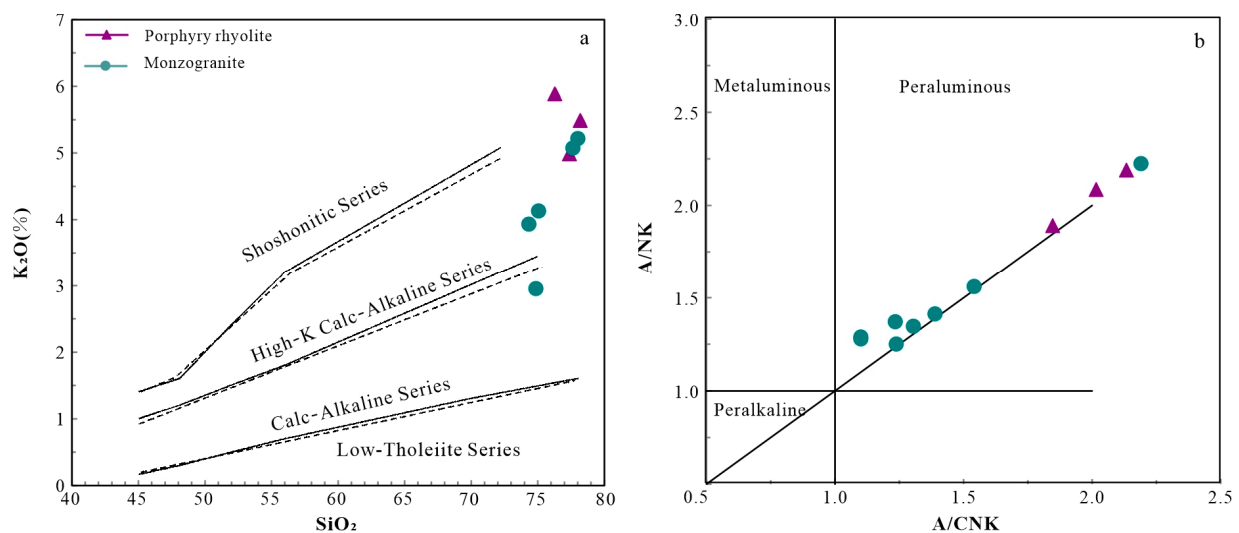


Figure 7. SiO_2 – K_2O (a) [33] and A/CNK–A/NK (b) [34] diagrams of monzogranites and rhyolitic porphyries in the Wunugetu deposit.

5.5. Rare Earth and Trace Elements

The rhyolite samples from the Wunugetu deposit showed total REE (ΣREE) contents ranging from 33.08 ppm to 78.07 ppm, LREE/HREE ratios between 13.70 and 15.96, and $(La/Yb)_N$ ratios from 21.48 to 31.23, indicating a general enrichment in light rare earth elements (LREEs) and a relative depletion in heavy rare earth elements (HREEs). Their chondrite-normalized REE patterns were rightward curves, with negative Eu anomalies ($Eu/Eu^* = 0.58$ – 0.75 ; Figure 8a; Table 3).

The monzogranite samples from the Wunugetu deposit yielded ΣREE contents from 61.57 ppm to 192.91 ppm, LREE/HREE ratios from 3.39 to 18.51, and $(La/Yb)_N$ ratios from 2.67 to 25.01, showing an enrichment in LREEs. Their chondrite-normalized REE patterns were also rightward curves, indicative of negative Eu anomalies ($Eu/Eu^* = 0.46$ – 0.75 ; Figure 8a; Table 3).

As revealed by the primitive mantle-normalized profiles, both rhyolitic porphyry and monzogranite samples exhibited similar patterns, both showing significant enrichment in LILEs such as Rb, K, Ba, and elements like Th, U, La, but depletion in HFSEs like Nb, P, and Ti (Figure 8b; Table 3). Both rock types had relatively low Sm/Nd ratios (rhyolitic porphyry: 0.17; monzogranite: 0.14 to 0.19, averaging 0.19), Rb/Sr ratios (rhyolitic porphyry: 1.64 to 2.70, averaging 2.24; monzogranite: 0.90 to 10.53, averaging 2.59), and Rb/Ba ratios (rhyolitic porphyry: 0.13 to 0.54, averaging 0.33; monzogranite: 0.13 to

0.30, averaging 0.20), along with higher K/Rb ratios (rhyolitic porphyry: 363.32 to 778.55, averaging 503.03; monzogranite: 200.48 to 658.60, averaging 353.81).

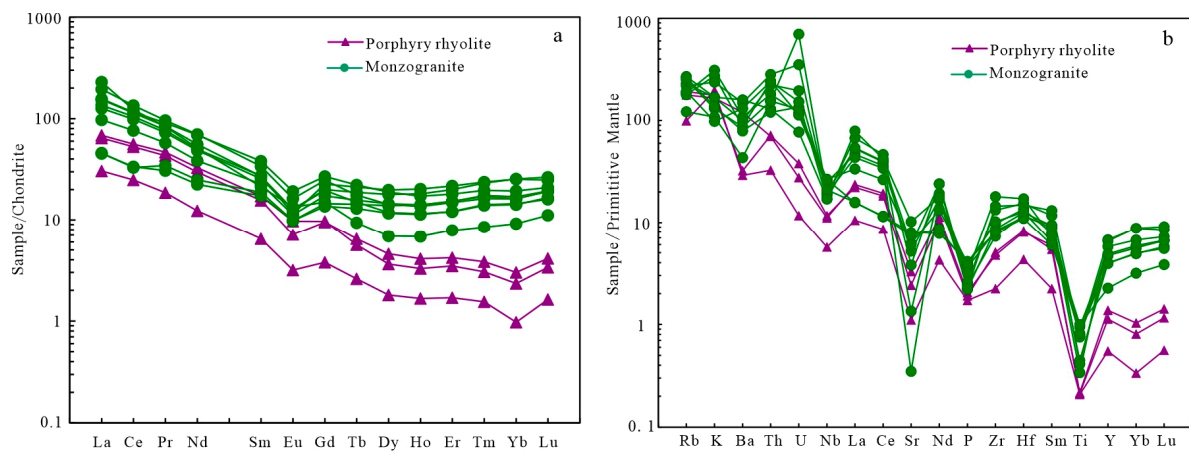


Figure 8. Chondrite-normalized REE patterns (a) [35] and spidergram of primitive mantle-normalized REEs (b) [36] of monzogranite and rhyolitic porphyries in the Wunugetu deposit.

6. Discussion

6.1. Diagenetic and Metallogenic Epochs

Mao Jingwen et al. (2005) proposed that metallization in eastern China predominantly occurred during the periods of 180–188 Ma, 135–144 Ma, 115–127 Ma, and 94–105 Ma [37]. Drawing from extensive isotopic dating data, Xu Wenliang et al. (2013) identified six distinct phases of mineralization-related volcanic activity in Northeast China: 220–280 Ma, 173–190 Ma, 158–166 Ma, 138–145 Ma, 106–133 Ma, and 88–97 Ma [38]. In the eastern Xing’an-Mongolia orogenic belt, principal metallization events are dated to 165–195 Ma and 110–115 Ma [39]. The Erguna block, a critical segment of the eastern CAOB, underwent notably intense Mesozoic magmatic episodes, categorized into seven stages: ~246 Ma (Late Permian to early Middle Triassic), ~225 Ma (late Middle Triassic to early Late Triassic), ~205 Ma (late Late Triassic to early Early Jurassic), ~185 Ma (Early Jurassic), ~155 Ma (Late Jurassic), ~137 Ma (early Early Cretaceous), and ~125 Ma (late Early Cretaceous) [40]. This block has revealed considerable porphyry copper mineralization, with several copper–molybdenum deposits like Badaguan, Taipingchuan, Wunugetu, and Naomingte in Mongolia being uncovered. Specifically, the Badaguan deposit’s quartz porphyries and granodiorite porphyries exhibit weighted average zircon U–Pb ages of 217.6 ± 2.6 Ma and 206.5 ± 1.6 Ma, respectively, while its molybdenite shows Re–Os ages of 222.4 ± 3.3 Ma [41,42]. The Taipingchuan deposit’s ore-forming granodiorite porphyries have average zircon U–Pb ages of 202.0 ± 5.7 Ma, with molybdenite revealing an average Re–Os age of 203 Ma [43]. In Mongolia’s Naomingte deposit, the ore-hosting granodiorites demonstrate a diagenetic age of 166 Ma. These findings suggest that the porphyry copper mineralization in the Erguna block primarily occurred from the Late Triassic to the Middle Jurassic, consistent with the Mesozoic magmatic activity timelines proposed by the aforementioned researchers.

The ore bodies in the Wunugetu deposit are primarily found within granite porphyries, monzogranites, quartz monzogranite porphyries, and biotite monzogranites, indicating a strong linkage with these rock types. Prior studies, leveraging isotopic geochronology, have suggested that the ore bodies and their encompassing rock masses share similar formation periods, highlighting Early Jurassic diagenesis and mineralization processes [13,15,44]. Contrarily, this study reveals that an ore-hosting monzogranite sample, WNG15, produced LA-ICP-MS zircon U–Pb ages of 209.0 ± 1.0 Ma, pointing to a late Late Triassic formation. Additionally, rhyolitic porphyries located in the northern part of the deposit, which intrude into the ore bodies without causing mineralization or alteration, implying that they are dykes intruding in the late mineralization stage. These rhyolitic porphyries

have shown LA-ICP-MS zircon U-Pb ages of 170.49 ± 0.81 Ma, indicating their formation during the early Middle Jurassic. The diverse ore features within the Wunugetu deposit imply a multi-stage mineralization process. Molybdenum mineralization predominantly occurs in joints and fissures, with the Re content in molybdenite being influenced by various factors such as lithology, paragenetic minerals, and temperature conditions [44,45]. Consequently, the molybdenite age may not precisely reflect the copper mineralization epoch. Considering the petrogenetic ages of monzogranite and rhyolitic porphyry in the deposit, along with chronological testing data on these rock masses obtained by previous researchers, the authors propose that the magmatic activity at Wunugetu Mountain spanned from 209.0 Ma to 170.5 Ma. When combined with the petrogenetic age range from 180 to 188 Ma for the ore-hosting monzogranitic porphyry in the deposit [15,17] and isochron ages of 177.4 to 179.8 Ma for the deposit's molybdenite [17,44], it can be inferred that the ore-bearing rock-bodies in the Wunugetu region were formed from the Late Triassic to the Early Jurassic, with the mineralization process predominantly occurring during the Early Jurassic.

6.2. Origins of Rocks and Source Characteristics

The genetic types of magmatic rocks are pivotal for interpreting the tectonic setting related to their origin and the characteristics of their magma sources. By examining mineral compositions and elemental geochemical traits, alongside considerations such as geotectonic context, variances in magma sources, and magma evolution, it is well-recognized that granitic rocks can be categorized into M, I, S, and A types [31,46,47]. In the case of the Wunugetu deposit under study, a microscopic analysis of monzogranite samples reveals the absence of key aluminous indicator minerals like cordierite, garnet, and muscovite, ruling out their classification as S-type granites [48]. The granitic rocks within the deposit and its vicinity are characterized by high silicon levels, potassium enrichment, and relatively high Th content. M-type granites, known to result from the remelting of the oceanic crust under island arcs, typically have mantle-derived magma sources, thus featuring low K_2O and Th contents [49,50], a stark contrast to the Late Triassic to Middle Jurassic rocks found in the Wunugetu deposit. Additionally, no contemporaneous M-type granites have been identified in the study area, indicating that the Mesozoic volcanic and magmatic rocks of the Wunugetu deposit are not M-type magmatic rocks. On the discrimination diagrams for magma origin (Figure 9a–c), the samples predominantly cluster around the I- and S-type granite zones, with only a couple aligning with the A-type granite category. Nonetheless, highly differentiated I- and S-type granitic samples with SiO_2 content exceeding 72% share similar geochemical characteristics to A-type magmatic rocks [47,51].

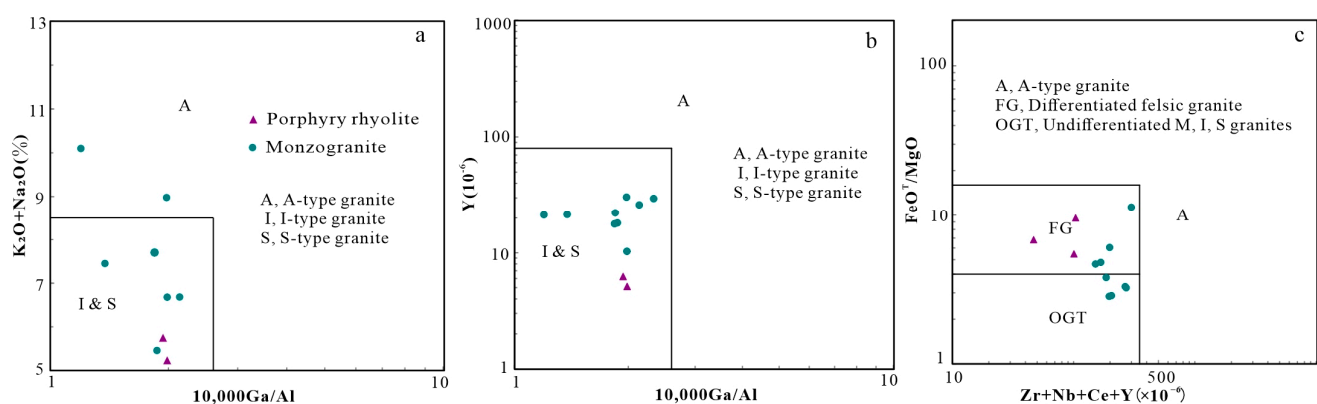


Figure 9. Identification of genetic types of monzogranites and rhyolitic porphyries in the Wunugetu deposit [47]. (a) $K_2O + Na_2O$ –Ga/Al diagram; (b) Y–Ga/Al diagram; (c) FeO^T/MgO –Zr + Nb + Ce + Y diagram.

The monzogranites within the Wunugetu deposit are characterized by high silicon content (73.16–80.47 wt.%), relatively low aluminum content (10.98–14.37 wt.%), enrichment in alkalis (3.42–10.10 wt.%), and depletion in magnesium and sodium, with A/CNK ratios ($\text{Al}_2\text{O}_3/(\text{CaO} + \text{Na}_2\text{O} + \text{K}_2\text{O})$) ranging from 1.1 to 2.9. On the A/NK–A/CNK diagram, the major element composition classifies these monzogranites as peraluminous to quasi-aluminous rocks. Additionally, these rocks, with low FeO^T , MgO, and CaO contents, are enriched in Rb and Th and depleted in Ba, P, and Ti (Figure 8b), indicative of significant crystallization and differentiation from primitive magmas [52,53]. The monzogranites also display low Zr + Nb + Ce + Y content (151.3 ppm–298.6 ppm, average: 198.6 ppm) and $10,000 \times \text{Ga}/\text{Al}$ ratios (1.20–2.33, average: 2.07), sharply contrasting with the typical characteristics of A-type granitic magmatic rocks (Zr + Nb + Ce + Y content: >400 ppm; $10,000 \times \text{Ga}/\text{Al}$ ratios: >2.6). As illustrated in the Zr + Nb + Ce + Y– FeO^T/MgO diagram (Figure 9c), most samples fell into the highly differentiated magma zone, indirectly confirming that the Wunugetu deposit's granitic rocks are highly differentiated magmatic rocks. Despite A/CNK ratios from 1.1 to 2.9 suggesting peraluminous to quasi-aluminous nature in the A/NK–A/CNK diagram, previous studies have substantiated that I-type magmatic rocks can exhibit peraluminous and even strongly peraluminous features [54,55]. As revealed by experiments, apatite exhibits low solubility and is prone to saturate undergoing fractional crystallization during magma evolution in I-type felsic magmas, with the P_2O_5 content diminishing with an increase in the SiO_2 content in rocks. Conversely, S-type granites have high apatite solubility, with P_2O_5 content increasing with the SiO_2 content [56]. Thus, the correlation between SiO_2 and P_2O_5 contents serves as a critical indicator for determining the type of granitic magma. As shown in the SiO_2 – P_2O_5 diagram (Figure 10a), the magmatic rock samples from the Wunugetu deposit exhibited low P_2O_5 content (0.04%–0.09%) and a negative P_2O_5 – SiO_2 correlation, classifying them as I-type granites. For S-type felsic magmas, Th and Y contents inversely correlate with Rb content, but in I-type magmas, they increase with Rb content [57]. Therefore, the evolutionary trends of Th and Y in magmas can be used to distinguish between S- and I-type granites. The positive correlation of the Th and Y contents with Rb content in the Rb–Y (Figure 10b) and Rb–Th (Figure 10c) diagrams indicates that the deposit's magmatic rocks are characteristic of I-type granites. The aforementioned microscopic observations reveal the absence of aluminum-rich silicate minerals like muscovite, cordierite, and garnet in monzogranites. All these lead to the conclusion that the Late Triassic magmatic rocks of the Wunugetu deposit are highly differentiated I-type rocks.

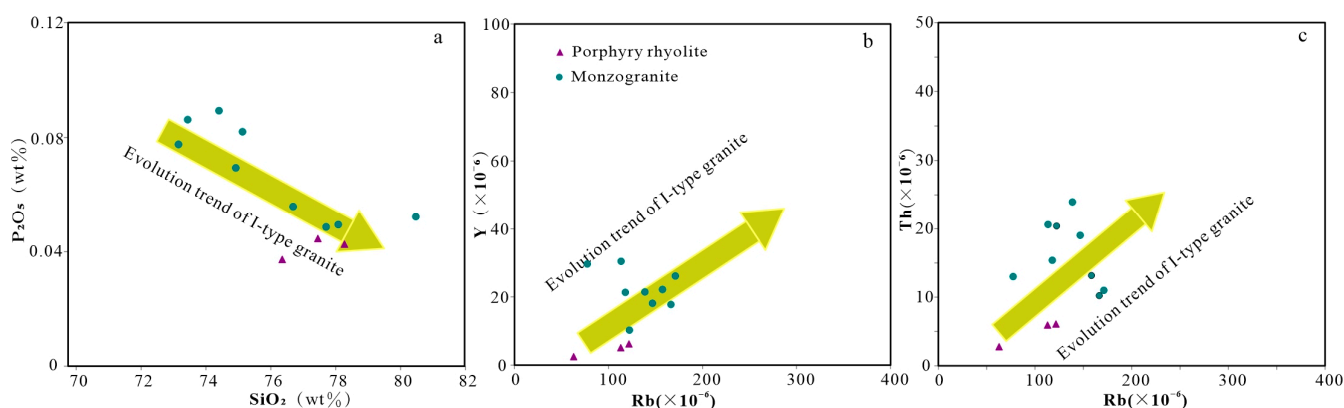


Figure 10. Diagrams of (a) SiO_2 – P_2O_5 , (b) of Rb–Y, (c) and Rb–Th of monzogranites and rhyolitic porphyries in the Wunugetu deposit [57].

The Middle Jurassic rhyolitic porphyry samples from the deposit all fell into the I- and S-type granite zones in the $10,000 \times \text{Ga}/\text{Al}$ vs. $\text{Na}_2\text{O} + \text{K}_2\text{O}$, $10,000 \times \text{Ga}/\text{Al}$ vs. Y, and Zr + Nb + Ce + Y vs. FeO^T/MgO diagrams. The Rb–Y (Figure 10b) and Rb–Th (Figure 10c)

diagrams, where Th and Y contents show a positive correlation with the Rb content, suggest that the rhyolite porphyries also have the geochemical characteristics of I-type granites.

These Middle Jurassic rhyolitic porphyries are characterized by high silica (75.77–77.45 wt.%), elevated potassium (5.005.91 wt.%), and an A/CNK ratio of 1.85 to 2.14, all above the 1.1 threshold. Their chondrite-normalized REE patterns exhibit pronounced HREE depletion, hinting at the potential residual effects of garnet. Positioned within the I- and S-type granite zones in geochemical diagrams like $(10,000 \times \text{Ga}/\text{Al})$ vs. $(\text{Na}_2\text{O} + \text{K}_2\text{O})$, $(10,000 \times \text{Ga}/\text{Al})$ vs. Y, and $(\text{Zr} + \text{Nb} + \text{Ce} + \text{Y})$ vs. $(\text{FeO}^{\text{T}}/\text{MgO})$ (Figure 10b,c), the samples also displayed an increase in P_2O_5 with SiO_2 in the SiO_2 vs. P_2O_5 diagram (Figure 10a), indicating that the rhyolite porphyries in the study area exhibit geochemical traits of S-type granites.

In-situ Lu-Hf isotopic analysis of zircon from these samples revealed $\epsilon_{\text{Hf}}(t)$ values between +2.4 and +7.6. Moreover, all these samples fell within the zone of the $\epsilon_{\text{Hf}}(t)$ range for CAOBS felsic rocks as shown in the t vs. $\epsilon_{\text{Hf}}(t)$ diagram (Figure 11a). Their T_{DM2} ages ranged from 727 to 1058 Ma, suggesting the rhyolitic porphyries' primitive magmas originated from the partial melting of the Meso- to Neoproterozoic accreted lower crust.

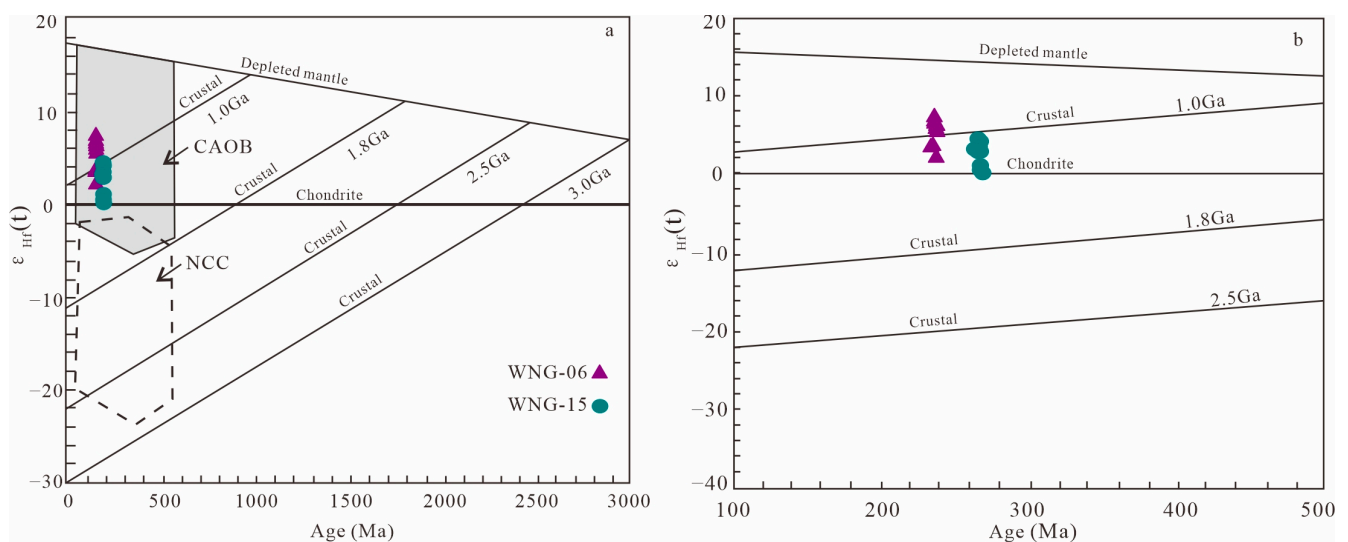


Figure 11. Hf isotopic characteristics (a), after Yang et al., 2006 [58] and $\epsilon_{\text{Hf}}(t)$ vs. U-Pb ages for zircons (b) of monzonites and rhyolitic porphyries from the Wunugetu deposit.

The Late Triassic monzogranite samples from the Wunugetu deposit yielded zircon $\epsilon_{\text{Hf}}(t)$ values ranging from +0.3 to +4.6. On the t - $\epsilon_{\text{Hf}}(t)$ diagram (Figure 11a), these samples clustered around the chondrite zone, displaying $\epsilon_{\text{Hf}}(t)$ values aligned with those of CAOBS felsic rocks. This suggests that the study area is a part of the CAOB. The T_{DM2} ages of these samples spanned 949 to 1227 Ma, indicating that the original magma of the rhyolite porphyries in the Wunugetu deposit is derived from partial melting of the Meso- to Neoproterozoic accreted lower crust.

In summary, both the Late Triassic I-type granites and the Early Jurassic rhyolitic porphyries from the Wunugetu deposit demonstrate positive zircon $\epsilon_{\text{Hf}}(t)$ values. These values show an increasing trend with a decrease in the emplacement age, suggesting that the magmatic source for the study area's monzogranites is derived from the partial melting of the Mesoproterozoic accreted lower crust.

6.3. Diagenetic and Metallogenic Tectonic Settings

The Wunugetu deposit, nestled within the eastern CAOB and the central MOSZ), is distinguished as the largest porphyry deposit in the Kherlen (Mongolia)-Erguna (China) block. Delving into the tectonic setting of rocks within this deposit is crucial for deepening our understanding of the MOSZ's tectonic evolution and contributes to the exploration

of the regional geological settings of porphyry copper mineralization and the tectonic evolution of the eastern CAOB. Previous studies on the evolution of the Mongol-Okhotsk Ocean generally indicate that this ocean evolved from the Eopaleozoic to the Mesozoic [59], undergoing bidirectional subduction toward the north and the south [22,60].

All samples of the Late Triassic magmatic rocks from the Wunugetu deposit fell within the volcanic arc-syn-collisional granite zone on the Y vs. Nb tectonic discrimination diagram (Figure 12a), with a majority situated within the volcanic arc granite zone on the Y + Nb – Rb diagram (Figure 12b). These Late Triassic magmatic rocks display the characteristics of I-type granites. It is believed that the highly differentiated I-type granites were formed in a subduction environment [61] or during the post-orogenic phase [62]. Considering their geochemical similarities with coeval magmatic rocks exposed in the northern Erguna block [40], this study posits that the study area was in an active continental margin environment subjected to subduction during the Late Triassic. This is associated with the southward subduction of the Mongol-Okhotsk Ocean sandwiched between the Neopaleozoic Siberian and Sino-Korean-Mongolian plates.

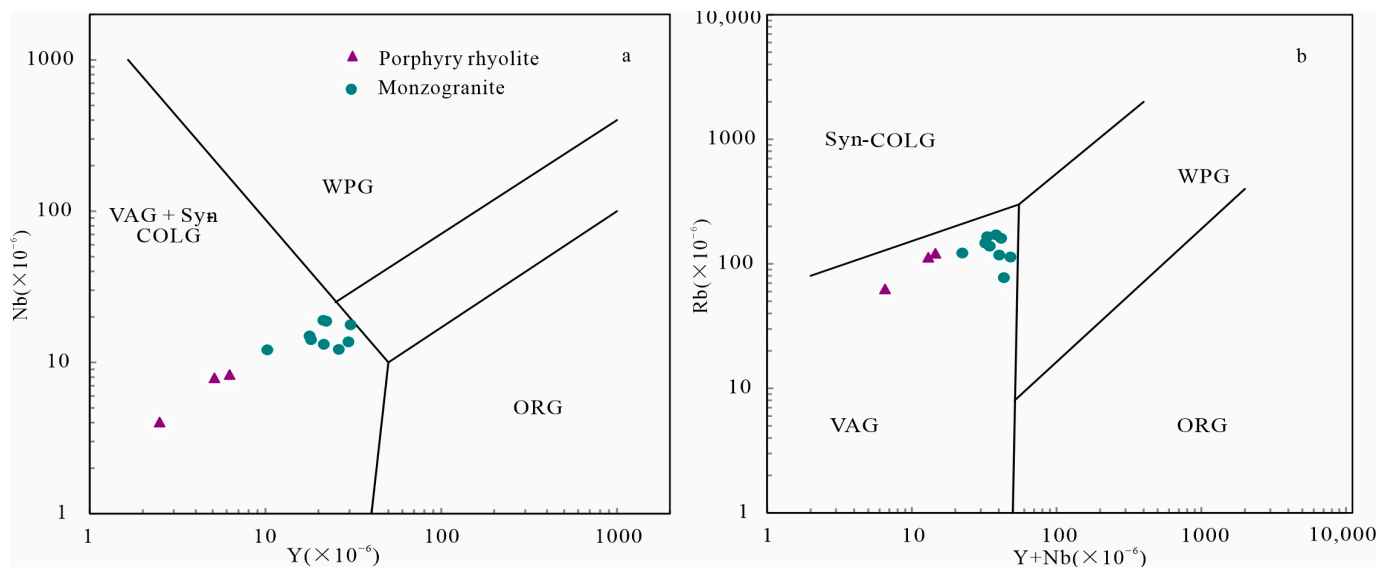


Figure 12. Diagrams of monzonites and rhyolitic porphyries from the Wunugetu deposit. (a) Y vs. Nb; (b) Y + Nb vs. Rb [63].

As illustrated by the Y-Nb tectonic discrimination diagram (Figure 12a), all samples of the Middle Jurassic rhyolitic porphyries from the Wunugetu deposit fall within the volcanic arc-syn-collisional granite zone. As shown in the Y + Nb vs. Rb (Figure 12b) and tectonic discrimination diagrams, these samples occupied the volcanic arc granite zone. Recent studies have unveiled a suite of Middle Jurassic (168 Ma) muscovite granites in the Sunwu area, adjacent to the study area. These granites originated from the partial melting of the thickened continental crust, resulting from the continent-continent collision during the closure of the Mongol-Okhotsk Ocean [64]. Additionally, the geochemical traits of the S-type granitic rhyolitic porphyry within the deposit suggest their formation in a continent-continent collisional context.

In summary, the geochemical characteristics of the monzogranites and rhyolitic porphyries in the Wunugetu deposit suggest that the Mongol-Okhotsk Ocean was still subjected to subduction during the Late Triassic. By the Middle Jurassic, following the ocean's closure, the ocean transitioned to a syn-collisional tectonic setting (Figure 13).

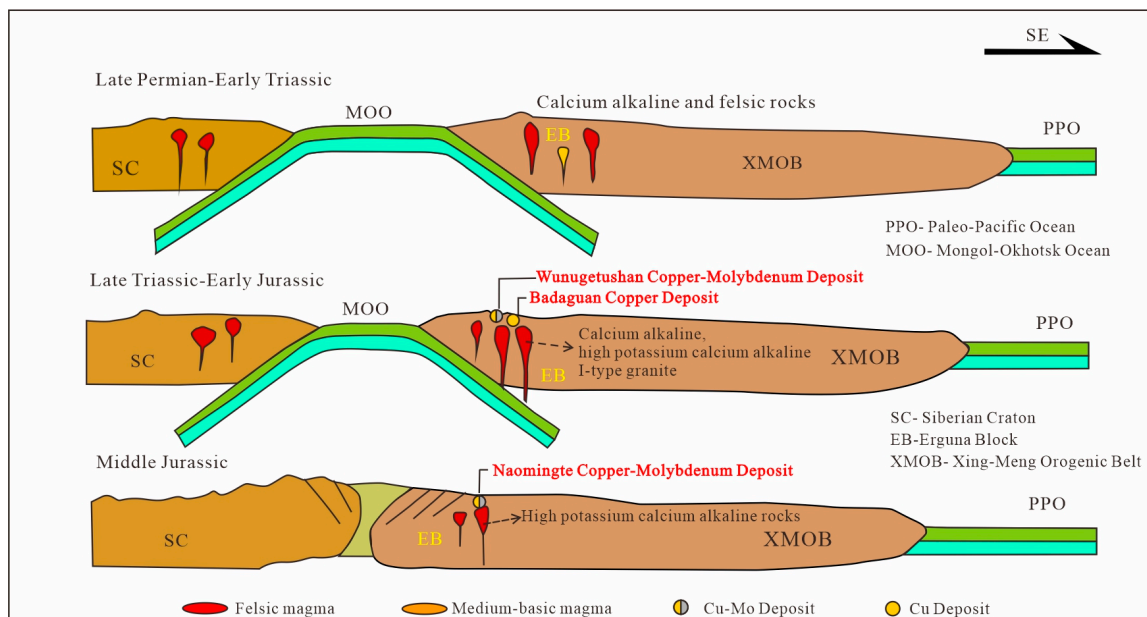


Figure 13. Diagram showing the evolutionary model of mineralization in the Mongolian-Okhotsk Ocean [65].

7. Conclusions

- (1) The formation age of the monzogranites in the Wunugetu deposit is established at 209.02 ± 1.0 Ma, while the rhyolitic porphyries are dated at 170.49 ± 0.81 Ma. This indicates that the deposit's magmatic activity primarily spanned from the Late Triassic to the Middle Jurassic, with the major ore-bearing intrusions dating from the Late Triassic to the Early Jurassic.
- (2) The Triassic monzogranites from the Wunugetu deposit exhibit the geochemical characteristics of I-type granites, including high silica and alkali content, enrichment in Rb and Th, and depletion in Ba, P, and Ti. The rhyolitic porphyries are characterized by high silica and potassium content, with trace elements exhibiting enrichment in LREEs and depletion in HREEs, aligning with the geochemical traits of S-type granites. Both the monzogranites and rhyolitic porphyries within the deposit exhibit positive zircon $\epsilon_{\text{Hf}}(t)$ values, indicating their source regions underwent the partial melting of juvenile crustal materials.
- (3) The Wunugetu porphyry copper–molybdenum deposit was formed within an active continental margin context, influenced by the southeastward subduction of the Mongol-Okhotsk Ocean from the Late Triassic to the Early Jurassic. Following the Mongol-Okhotsk Ocean's closure during the Middle Jurassic, the Wunugetu region transitioned to a syn-collisional tectonic setting.

Author Contributions: Conceptualization, Q.W. and Y.Y.; methodology, Q.W.; validation, Y.Y., Q.F. and Z.Z.; formal analysis, Q.W., Q.F., Z.Z. and X.G.; investigation, Z.Z., X.G., T.W., L.C. and Y.Z.; data curation, Q.W.; writing—original draft preparation, Q.W.; writing—review and editing, Y.A.; supervision, Y.Y.; project administration, Q.F.; funding acquisition, Y.Y. All authors have read and agreed to the published version of the manuscript.

Funding: This work was supported by the Investigation and Evaluation of Copper and Lithium Resources in Mongolia (No. DD20230586) from the China Geological Survey, the Northeast Geological Science and Technology Innovation Center Regional Innovation Fund (No. QCJJ2022-38).

Data Availability Statement: The data presented in this study are available in Tables 1–3.

Acknowledgments: The authors express their deep gratitude towards the two anonymous reviewers and the academic editor for their insightful and invaluable suggestions.

Conflicts of Interest: Qiulin Fu is an employee of Liaoning Province Institute of Geology and Mineral Resources Co., Ltd. and Xiaodan Guo is an employee of Liaoning Province Geology and Mineral Group Energy Geology Co., Ltd. We declare that we have no financial and personal relationships with other people or organizations that can inappropriately influence our work, there is no professional or other personal interest of any nature or kind in any product, service and/or company that could be construed as influencing the position presented in, or the review of, the manuscript entitled.

References

1. Sengör, A.M.C.; Natal'in, B.A.; Burtman, V.S. Evolution of the Altaid tectonic collage and Palaeozoic crustal growth in Eurasia. *Nature* **1993**, *364*, 299–307. [[CrossRef](#)]
2. Jahn, B.M.; Wu, F.Y.; Chen, B. Massive granitoid generation in Central Asia: Nd isotope evidence and implication for continental growth in the Phanerozoic. *Episodes* **2000**, *23*, 82–92. [[CrossRef](#)]
3. Jahn, B.M.; Wu, F.Y.; Chen, B. Granitoids of the Central Asian Orogenic Belt and continental growth in the Phanerozoic. *Earth and Environ. Sci. Trans. R. Soc. Edinb.* **2000**, *91*, 181–193.
4. Badarch, G.; Cunningham, W.D.; Windley, B.F. A new terrane subdivision for Mongolia: Implications for the Phanerozoic crustal growth of central Asia. *J. Asian Earth Sci.* **2002**, *21*, 87–110. [[CrossRef](#)]
5. Buslov, M.M.; Saphonova, I.Y.; Watanabe, T.; Obut, O.T.; Fujiwara, Y.; Iwata, K.; Sugai, Y.; Smirnova, L.V.; Kazansky, A.Y. Evolution of the Paleo-Asian Ocean (Altai–Sayan region, Central Asia) and collision of possible Gondwana-derived terranes with the southern marginal part of the Siberian continent. *Geosci. J.* **2001**, *5*, 203–224. [[CrossRef](#)]
6. Windley, B.F.; Alexeiev, D.; Xiao, W.J.; Kröner, A.; Badarch, G. Tectonic models for accretion of the Central Asian Orogenic Belt. *J. Geol. Soc.* **2007**, *164*, 31–47. [[CrossRef](#)]
7. Wu, F.Y.; Sun, D.Y.; Ge, W.C.; Zhang, Y.B.; Grant, M.L.; Wilde, S.A.; Jahn, B.M. Geochronology of the Phanerozoic granitoids in northeastern China. *J. Asian Earth Sci.* **2011**, *41*, 1–30. [[CrossRef](#)]
8. Cai, K.D.; Sun, M.; Yuan, C.; Zhao, G.C.; Xiao, W.J.; Long, X.P.; Wu, F.Y. Carboniferous mantle-derived felsic intrusion in the Chinese Altai, NW China: Implications for geodynamic change of the accretionary orogenic Belt. *Gondwana Res.* **2012**, *22*, 681–698. [[CrossRef](#)]
9. Tu, G.Z. Preliminary discussion on the Central Asian metallogenic domain. *Geol. Sci.* **1999**, *34*, 397–404, (In Chinese with English abstract).
10. Xiao, W.; Song, D.; Windley, B.F.; Li, J.; Han, C.; Wan, B.; Zhang, J.; Ao, S.; Zhang, Z. Research progresses of the accretionary processes and metallogenesis of the Central Asian Orogenic Belt. *Sci. China Earth Sci.* **2019**, *11*, 14–19, (In Chinese with English abstract).
11. Wang, Q.S.; Wei, Y.L.; Gao, J.; Xiong, X.L.; Wang, J.B.; Guo, Z.J.; Li, J.T.; Sun, M. Zircon U–Pb ages and geochemistry of granitoid in the Yuejinshan copper–gold deposit, NE China: Constraints on the petrogenesis and metallogenesis. *Minerals* **2021**, *11*, 1206. [[CrossRef](#)]
12. Wang, Z.T.; Qin, K.Z. Geological and geochemical feature and the source of metallogenetic matter of lower crust porphyry Cu–Mo deposit in Wunugetu Mountain. *Min. Depos.* **1988**, *7*, 3–15, (In Chinese with English abstract).
13. Tan, G. *Research on the Ore-Forming Process of the Wunugetu Porphyry Copper Molybdenum Deposit in Inner Mongolia*; Chinese Academy of Geological Sciences: Beijing, China, 2011; (In Chinese with English abstract).
14. Li, N. *The Characteristics and Mineralization Age of Intrusive Rocks in the Wunugetu Copper Molybdenum Deposit, Inner Mongolia*; China University of Geosciences: Beijing, China, 2013; (In Chinese with English abstract).
15. Qin, K.Z.; Li, H.M.; Li, W.S.; Ishihara, S. Diagenesis and Metallogenic Era of Wunugetu Porphyry Copper Molybdenum Deposit in Inner Mongolia. *Geol. Rev.* **1999**, *2*, 180–185, (In Chinese with English abstract).
16. Chen, Z.G.; Zhang, L.C.; Wan, B.; Zhang, Y.T.; Wu, H.Y. Geochemical characteristics and geological significance of low Sr Yb type ore-forming porphyry in the Wunugetu porphyry copper molybdenum deposit, Inner Mongolia. *Acta Petrol. Sin.* **2008**, *24*, 115–128, (In Chinese with English abstract).
17. Tan, G.; Chang, G.X.; She, H.Q.; Li, J.W.; Zhang, D.Q.; Yang, X.C.; Zhang, B.; Xiang, A.P.; Dong, Y.J. Rhenium osmium isotope dating of molybdenite in Wunugetu porphyry copper molybdenum deposit, Inner Mongolia and its geological significance. *Miner. Depos.* **2010**, *29*, 506–508, (In Chinese with English abstract).
18. Chen, Z.G.; Zhang, L.C.; Wan, B.; Wu, H.Y.; Cleven, N. Geochronology and geochemistry of the Wunugetu porphyry Cu–Mo deposit in NE China, and their geological significance. *Ore Geol. Rev.* **2011**, *43*, 92–105. [[CrossRef](#)]
19. Sengör, A.M.C.; Natal'in, B.A. Paleotectonics of Asia: Fragments of a synthesis. In *The Tectonic Evolution of Asia*; Yin, A., Harrison, T.M., Eds.; Cambridge University Press: Cambridge, UK, 1996; pp. 486–641.
20. Li, J.Y. Permian geodynamic setting of Northeast China and adjacent regions: Closure of the Paleo-Asian ocean and subduction of the Paleo-Pacific plate. *J. Asian Earth Sci.* **2006**, *26*, 207–224. [[CrossRef](#)]
21. Tang, J.; Xu, W.L.; Wang, F.; Zhao, S.; Wang, W. Early Mesozoic southward subduction history of the Mongol–Okhotsk oceanic plate: Evidence from geochronology and geochemistry of Early Mesozoic intrusive rocks in the Erguna Massif, NE China. *Gondwana Res.* **2016**, *31*, 218–240. [[CrossRef](#)]

22. Tang, J.; Xu, W.L.; Wang, F.; Wang, W.; Xu, M.J.; Zhang, Y.H. Geochronology and geochemistry of Early–Middle Triassic magmatism in the Erguna Massif, NE China: Constraints on the tectonic evolution of the Mongol–Okhotsk Ocean. *Lithos* **2014**, *184–187*, 1–16. [[CrossRef](#)]
23. Li, Y.; Xu, W.L.; Wang, F.; Tang, J.; Zhao, S.; Guo, P. Geochronology and geochemistry of late Paleozoic–early Mesozoic igneous rocks of the Erguna Massif, NE China: Implications for the early evolution of the Mongol–Okhotsk tectonic regime. *J. Asian Earth Sci.* **2017**, *144*, 205–224. [[CrossRef](#)]
24. Hou, Z.S. *The Genesis and Tectonic Background of the Badaguan Copper Molybdenum Deposit in the Erguna Area of Inner Mongolia*; Jilin University: Changchun, China, 2014; (In Chinese with English abstract).
25. Niu, S.D. *Magmatic Intrusion Sequence and Mineralization of the Jiawula Lead-Zinc Silver Deposit in the Daxing’anling Mountains*; China University of Geosciences: Beijing, China, 2017; (In Chinese with English abstract).
26. Wiedenbeck, M.; Allé, P.; Corfu, F.; Griffin, W.L.; Meier, M.; Oberli, F.; von Quadt, A.; Roddick, J.C.; Spiegel, W. Three natural zircon standards for U–Th–Pb, Lu–Hf, trace element and REE analyses. *Geostand. Newsl.* **1995**, *19*, 1–23. [[CrossRef](#)]
27. Slama, J.; Košler, J.; Condon, D.J.; Crowley, J.L.; Gerdes, A.; Hanchar, J.M.; Horstwood, M.S.A.; Morris, G.A.; Nasdala, L.; Norberg, N.; et al. Plešovice zircon—A new natural reference material for U–Pb and Hf isotopic microanalysis. *Chem. Geol.* **2008**, *249*, 1–35. [[CrossRef](#)]
28. Liu, Y.S.; Hu, Z.C.; Zong, K.Q.; Gao, C.G.; Gao, S.; Xu, J.; Chen, H.H. Reappraisal and refinement of zircon U–Pb isotope and trace element analyses by LA-ICP-MS. *Chin. Sci. Bull.* **2010**, *55*, 1535–1546. [[CrossRef](#)]
29. Ludwig, K.R. *Isoplot/Ex Version 3.00: A Geochronological Toolkit for Microsoft Excel*; Berkeley Geochronology Center: Berkeley, CA, USA, 2003.
30. Andersen, T. Correction of Common Lead in U–Pb Analyses that Do Not Report ²⁰⁴Pb. *Chem. Geol.* **2002**, *192*, 59–79. [[CrossRef](#)]
31. Wu, F.Y.; Li, X.H.; Zheng, Y.F.; Gao, S. Lu–Hf isotopic systematics and their applications in petrology. *Acta Petrol. Sin.* **2007**, *23*, 185–220. (In Chinese with English abstract).
32. Middlemost, E.A.K. Naming materials in the magma/igneous rock system. *Earth Sci. Rev.* **1994**, *37*, 215–224. [[CrossRef](#)]
33. Peccerillo, R.; Taylor, S.R. Geochemistry of eocene calc-alkaline volcanic rocks from the Kastamonu area, Northern Turkey. *Contrib. Miner. Petrol.* **1976**, *58*, 63–81. [[CrossRef](#)]
34. Maniar, P.D.; Piccoli, P.M. Tectonic discrimination of granitoids. *Geol. Soc. Am. Bull.* **1989**, *101*, 635–643. [[CrossRef](#)]
35. Boynton, W.V. Geochemistry of the rare earth elements: Meteorite studies. In *Rare earth Element Geochemistry*; Henderson, P., Ed.; Elsevier: Amsterdam, The Netherlands, 1984; pp. 63–114.
36. Sun, S.S.; McDonough, W.F. Chemical and Isotopic Systematics of Oceanic Basalts: Implications for Mantle Composition and Processes. *Geol. Soc. Lond. Spec. Publ.* **1989**, *42*, 313–345. [[CrossRef](#)]
37. Mao, J.W.; Xie, G.Q.; Zhang, Z.H.; Li, X.F.; Wang, Y.T.; Zhang, C.Q.; Li, Y.F. Mesozoic large-scale metallogenic pulses in North China and corresponding geodynamic settings. *Acta Petrologica Sin.* **2005**, *21*, 169–188.
38. Xu, W.L.; Wang, F.; Pei, F.P.; Meng, E.; Tiang, J.; Xu, M.J.; Wang, W. Mesozoic tectonic regimes and regional ore-forming background in NE China: Constraints from spatial and temporal variations of Mesozoic volcanic rock associations. *Acta Petrol. Sin.* **2013**, *29*, 339–353.
39. Sun, J.G.; Zhang, Y.; Xing, S.W.; Zhao, K.Q.; Zhang, Z.J.; Bai, L.A.; Ma, Y.B.; Liu, Y.S. Genetic types ore-forming age and geodynamic setting of endogenic molybdenum deposits in the eastern edge of Xing-Meng orogenic belt. *Acta Petrologica Sin.* **2012**, *28*, 1317–1332.
40. Tang, J. *Chronology and Geochemistry of Mesozoic Igneous Rocks in the Erguna Block: Constraints on the Tectonic Evolution of the Mongolian Okhotsk Suture Zone*; Jilin University: Changchun, China, 2016; (In Chinese with English abstract).
41. Zhang, J.; Shao, J.; Zhou, Y.H.; Bao, Q.Z.; Wang, H.B. Geochemical characteristics and U–Pb, Re–Os ages of the Badaguan copper molybdenum deposit in Chenbalhu Banner, Inner Mongolia. *Geol. Bull. China* **2016**, *35*, 1388–1399. (In Chinese with English abstract).
42. Wang, X.; Duan, M.X.; Ren, Y.S.; Hou, Z.S.; Sun, D.Y.; Hao, Y.J. Fluid Inclusion Characteristics and Metallogenic Era of the Badaguan Copper Molybdenum Deposit in the Erguna Area of Inner Mongolia. *J. Jilin Univ. (Earth Sci. Ed.)* **2016**, *46*, 1354–1367. (In Chinese with English abstract).
43. Chen, Z.G.; Zhang, L.C.; Lu, B.Z.; Li, Z.L.; Wu, H.Y.; Xiang, P.; Huang, S.W. Geochronology and Geochemistry of the Taipingshan Copper–Molybdenite Deposit in Inner Mongolia, and Its Geological Significances. *Acta Petrol. Sinica* **2010**, *26*, 1437–1449. (In Chinese with English abstract).
44. Wang, Y.H.; Zhao, C.B.; Zhang, F.F.; Liu, J.J.; Wang, J.P.; Peng, R.M.; Liu, B. SIMS zircon U–Pb and molybdenite Re–Os geochronology, Hf isotope, and whole-rock geochemistry of the Wunugetu porphyry Cu–Mo deposit and granitoids in NE China and their geological significance. *Gondwana Res.* **2015**, *28*, 1228–1245. [[CrossRef](#)]
45. Yang, Z.F.; Luo, Z.H.; Lu, X.X.; Cheng, L.L.; Huang, F. Discussion on the Tracer Sources of Re Content in Molybdenum Ores. *Miner. Depos.* **2011**, *30*, 654–674. (In Chinese with English abstract).
46. Chappell, B.W.; White, A.J.R. Two contrasting granite types. *Pac. Geol.* **1974**, *8*, 173–174.
47. Whalen, J.B.; Currie, K.L.; Chappell, B.W. A-type granites: Geochemical characteristics, discrimination and petrogenesis. *Contrib. Mineral. Petrol.* **1987**, *95*, 407–419. [[CrossRef](#)]
48. Pitcher, W.S. *The Nature and Origin of Granite*, 2nd ed.; Springer: Dordrecht, The Netherlands, 1997.

49. Chen, J.L.; Guo, Y.S.; Fu, S.M. Progress in Granite Research—Overview of ISMA Granite Classification. *Gansu Geol.* **2004**, *13*, 67–73, (In Chinese with English abstract).
50. Freund, S.; Haase, K.M.; Keith, M.; Beier, C.; Garbe-Schönberg, D. Constraints on the formation of geochemically variable plagiogranite intrusions in the Troodos Ophiolite, Cyprus. *Contrib. Mineral. Petrol.* **2014**, *167*, 978. [[CrossRef](#)]
51. Wu, F.Y.; Jahn, B.M.; Wilde, S.A.; Lo, C.H.; Yui, T.F.; Lin, Q.; Ge, W.C.; Sun, D.Y. Highly fractionated I-type granites in NE China (I): Geochronology and petrogenesis. *Lithos* **2003**, *66*, 241–273. [[CrossRef](#)]
52. Sylvester, P.J. Post-collisional strongly peraluminous granites. *Lithos* **1998**, *45*, 29–44. [[CrossRef](#)]
53. Clemens, J.D. S-type granitic magmas-petrogenetic issues, models and evidence. *Earth-Sci. Rev.* **2003**, *61*, 1–18. [[CrossRef](#)]
54. Sisson, T.W.; Ratajeski, K.; Hankins, W.B.; Glazner, A.F. Voluminous granitic magmas from common basaltic sources. *Contrib. Mineral. Petrol.* **2005**, *148*, 635–661. [[CrossRef](#)]
55. Chappell, B.W.; Bryant, C.J.; Wyborn, D. Peraluminous I-type granites. *Lithos* **2012**, *153*, 142–153. [[CrossRef](#)]
56. Watson, E.B.; Capobianco, C.J. Phosphorus and the rare earth elements in felsic magmas: An assessment of the role of apatite. *Geochim. Cosmochim. Acta* **1981**, *45*, 2349–2358. [[CrossRef](#)]
57. Chappell, B.W. Aluminium saturation in I- and S-type granites and the characterization of fractionated haplogranites. *Lithos* **1999**, *46*, 535–551. [[CrossRef](#)]
58. Yang, J.H.; Wu, F.Y.; Shao, J.A.; Wilde, S.A.; Xie, L.W.; Liu, X.M. Constraints on the timing of uplift of the Yanshan fold and thrust belt, North China. *Earth Planet. Sci. Lett.* **2006**, *246*, 336–352. [[CrossRef](#)]
59. Xu, W.L.; Sun, C.Y.; Tang, J.; Luan, J.P.; Wang, F. Basement nature and tectonic evolution of the Xing’an-Mongolian orogenic belt. *Earth Sci.* **2019**, *44*, 1620–1646, (In Chinese with English abstract).
60. Xu, W.L.; Pei, F.P.; Wang, F.; Meng, E.; Ji, W.Q.; Yang, D.B.; Wang, W. Spatial-temporal relationships of Mesozoic volcanic rocks in NE China: Constraints on tectonic overprinting and transformations between multiple tectonic regimes. *J. Asian Earth Sci.* **2013**, *74*, 167–193. [[CrossRef](#)]
61. Zhu, D.C.; Mo, X.X.; Wang, L.Q.; Zhao, Z.D.; Niu, Y.L.; Zhou, C.Y.; Yang, Y.H. Genesis of the Chayu highly differentiated I-type granite in eastern Gangdise, Xizang: Zircon U-Pb geochronology, geochemistry and Sr Nd Hf isotope constraints. *Sci. Sin. (Terrae)* **2009**, *39*, 833–848, (In Chinese with English abstract).
62. Wu, F.Y.; Liu, X.C.; Ji, W.Q.; Wang, J.M.; Yang, L. Highly fractionated granites: Recognition and research. *Sci. China (Earth Sci.)* **2017**, *60*, 1201–1219. [[CrossRef](#)]
63. Pearce, J.A.; Harris, N.B.W.; Tindle, A.G. Trace element, discrimination diagrams for the tectonic interpretation of granitic rocks. *J. Petrol.* **1984**, *25*, 956–983. [[CrossRef](#)]
64. Li, Y.; Ding, L.L.; Xu, W.L.; Wang, F.; Tang, J.; Zhao, S.; Wang, Z.J. Chronology and geochemistry of the Middle Jurassic muscovite granite in the Sunwu area: Constraints on the closure time of the Mongol-Okhotsk Ocean. *Acta Petrol. Sin.* **2015**, *31*, 56–66.
65. Han, R.; Qin, K.Z.; Su, S.Q.; Groves, D.I.; Zhao, C.; Hui, K.X.; Meng, Z.J. An Early Cretaceous Ag-Pb-Zn mineralization at Halasheng in the South Erguna Block, NE China: Constraints from U-Pb and Rb-Sr geochronology, geochemistry and Sr-Nd-Hf isotopes. *Ore Geol. Rev.* **2020**, *122*, 103526. [[CrossRef](#)]

Disclaimer/Publisher’s Note: The statements, opinions and data contained in all publications are solely those of the individual author(s) and contributor(s) and not of MDPI and/or the editor(s). MDPI and/or the editor(s) disclaim responsibility for any injury to people or property resulting from any ideas, methods, instructions or products referred to in the content.